Master's thesis

NTNU
Norwegian University of Science and Technology
Department of Ocean Operations and Civil Engineering

Jesper van der Meij

Wave Response Experiments of Fish Farms

Master's thesis in Naval Architecture
Supervisor: Karl Henning Halse
Co-supervisor: Henry Piehl
June 2023

NTNU
Norwegian University of
Science and Technology

Jesper van der Meij

Wave Response Experiments of Fish Farms

Master's thesis in Naval Architecture
Supervisor: Karl Henning Halse
Co-supervisor: Henry Piehl
June 2023

Norwegian University of Science and Technology
Department of Ocean Operations and Civil Engineering

NTNU
Norwegian University of
Science and Technology

Preface

This thesis has been written as the conclusion of a two year master's programme in Naval Architecture at the Norwegian University of Science and Technology (NTNU) in Ålesund, Norway. The research consisted of reviewing literature on aquaculture, setting up a wave height measurement system at the model tank, creating a digital and physical model of a fish farm, and carrying out model tank experiments to examine the wave motion response of the model.

The intended audience is anyone with an interest in fish farming, water waves, and/or doing experiments in model tanks. It is expected the reader has basic knowledge of the mathematics and physics used in engineering. However, a theoretical background is provided at the start of each chapter and relevant sources with more information are referred to.

The main motivation for choosing this topic is an interest in the aquaculture sector, as I believe the sustainable growth of this sector will contribute to creating healthy food for the world's growing population. I have also been involved in developing the other systems at the model tank, and I believe that doing practical things like these model tests is a great way to find improvements that can be made to the tank.

The thesis is structured as follows: Chapter 1 gives background information on aquaculture and puts the research into perspective. It also details the objectives and scope of the research. Chapter 2 is about the research into the wave environment in the model tank. Chapter 3 describes how the physical and digital model were created and presents the result of the digital simulation. Chapter 4 explains the main experiment, illustrates the sensor setup, and presents the result of the model tests. Finally, Chapter 5 brings all the results together and provides the conclusions, discussion, and recommendations for further work.

All that said, I would like to thank Karl Henning Halse for helping define the subject, his guidance during the research, and providing the software used for the digital model. Next, thanks to Henry Piehl for his enthusiasm with the experiments, tedious work in setting up the sensors, and helping with signal processing. Thanks also goes out to friends and family for proof-reading. In particular Mara Bakker for her valuable comments and mental support, and Håkon Fallmyr for helping with the Norwegian summary. Lastly, a shout-out to Wikipedia user Kraaiennest, who wrote basically the entire encyclopedia collection on water waves.

Jesper van der Meij

Ålesund, 06.06.2023

This page was left blank intentionally

Thesis agreement

Background

Established fish farm designs require a sheltered area with a steady water current for nutrients and waste disposal. The growth of the aquaculture industry has caused a shortage of these ideal locations, and has required farms to be built in more exposed locations. Furthermore, farm designs are larger and use new technologies to house more fish.

These developments cause the motions and loads of the structure to be very different. While there is little information found on testing procedures, it is expected that rules and regulations on the analysis of new farms will become stricter in the coming years. Examining the motion response of a farm with various cage configurations will provide insight for wave- fish cage interaction and help to improve the design for wave environment conditions.

Objectives and scope

The primary objective of the study is to carry out model tank experiments to study fish farm motions in waves. The newly installed motion tracking system at NTNU in Ålesund presents an opportunity in relation to this objective. The milestones in this study are as follows:

- Obtain an understanding of the wave characteristics in the model tank at NTNU in Ålesund
- Define a test procedure for carrying out wave response experiments
- Create a computer simulation model to validate experiments
- Analyse the motion response of various farm designs with model tank experiments

The wave tank introduces limitations on the dimensions of the model and waves, which must be examined. Doing experiments on model scale introduces limitations in the accuracy of the model, as some aspects cannot be modelled accurately.

Approach

1. Create and install a system for measuring the wave height in the tank
2. Identify and select suitable instrumentation of tank and model
3. Establish an understanding of wave characteristics in the tank and figure out what waves are viable representations of real life conditions
4. Define a base case and different cage designs to be tested, wave height & period
5. Perform the computer simulation
6. (parallel) Create a prototype model to find viable dimensions of measured model
7. Design a floater ring and mooring system which can contain all different net types
8. Carry out model tank experiments

The scope of work may prove to be larger than initially anticipated. Subject to approval from the advisor, topics from the list above may be deleted or reduced in extent.

The thesis should be written as a research report with summary, conclusion, literature references, table of contents, etc. During preparation of the text, the candidate should make efforts to create a well arranged and well written report. To ease the evaluation of the thesis, it is important to cross-reference text, tables and figures. For evaluation of the work a thorough discussion of results is needed. Discussion of research method, validation and generalization of results is also appreciated.

The thesis shall be submitted in electronic version according to standard procedures. Instructions are found on the NTNU website (Inspera) and on Blackboard. In addition, one paper copy of the full thesis together with an electronic device carrying all relevant documents and files shall be submitted to your supervisor.

Delivery: 08.06.2023

Abstract

The global aquaculture industry is in a phase of steady expansion. The sustainable growth of the aquaculture sector is a great opportunity to secure healthy food for many. Ensuring sustainability requires strict rules and regulations, which benefit from extensive testing of new designs and production procedures. Creating an experimental setup and measuring the wave motion response of a fish farm in the model tank at NTNU in Ålesund shows that it is possible to conduct these experiments at a relatively small facility.

Wave tests with a range of wave periods and wave steepness were carried out in the model tank. Regular waves were created using a single-flap wave maker at one end of the tank. The resulting wave height was measured using a wave probe and the measurements were compared to linear and second-order wave theory. A physical model of a fish farm with an assumed model scale of 1:75 was created using widely available materials. The model was moored in the model tank and subjected to regular waves with the same period range as in the wave tests. The vertical motion of the model was measured using a motion-tracking camera system, and the frequency response characteristics were obtained. The results were compared to a digital simulation in the same scale as the physical model.

The wave tests showed that when the wave steepness increases, second-order theory becomes increasingly important. Furthermore, it became clear that none of the waves reached their theoretical wave height. It appeared this effect is mostly dependent on the wave period. It is suspected that the wave flap itself is the main source of inaccuracies in the waves. The model tests and digital simulation both showed a frequency response characteristic that correlates with the theory on the response of floating structures. However, the results did not correspond to each other. It is suspected that this is mainly due to the stiffness parameters of both models, which were not researched.

It is concluded that conducting wave response experiments in the model tank at NTNU in Ålesund is possible. However, further research into the wave environment and model parameters is required to obtain accurate, reproducible results.

This page was left blank intentionally

Sammendrag

Den globale havbruksnæringen er i en fase med store expansjon. Bærekraftig vekst i havbrukssektoren er en flott mulighet til å sikre sunn mat for mange. Det krever strenge regler og forskrifter, som drar nytte av omfattende testing av nye design og produksjonsprosedyrer. Å lage et forsøksoppsett og måle bølgeresponsen til et oppdrettsanlegg i modelltanken ved NTNU i Ålesund viser at det er mulig å gjennomføre disse forsøkene på et relativt lite anlegg.

Bølgetester med en rekke perioder og bratthet ble utført i modelltanken. Regulære bølger ble generert ved hjelp av en bølgemaker i den ene enden av tanken. Den resulterende bølgehøyden ble målt og sammenlignet med lineær og andreordens bølgeteori. En modell av et oppdrettsanlegg med en antatt modellskala på 1:75 ble laget ved bruk av tilgjenlige materialer. Modellen ble fortøyd i modelltanken og utsatt for regulære bølger med samme perioderområde som i bølgetestene. Den vertikale bevelgelsen til modellen ble målt av et kamerasystem og frekvensrespons ble opnådd. Resultatene ble sammenlignet med en digital simulering i samme skala som den fysiske modellen.

Bølgetestene viste at når bølgebrattheten øker, blir andreordens teori stadig viktigere. Videre ble det klart at ingen av bølgene nådde sin teoretiske bølgehøyde. Det så ut til at denne effekten hovedsakelig er avhengig av bølgeperioden. Det er en mistanke om at selve bølgemakeren er hovedkilden til unøyaktigheter i bølgene. Modelltestene og digital simulering viste begge en frekvensreponskarakterestikk som korrelere med teorien om responsen til flyttende inretninger. Resultatene samsvarte imidlertid ikke med hverandere, og det er mistanke om at dette hovedsakelig skyldes stivhetsparametrene til modellene, som ikke ble undersøkt.

Det konkluderes med at det er mulig å gjennomføre bølgeresponsforsøk i modelltanken ved NTNU i Ålesund. Videre forskning på bølgemiljøet og modellparameterene er imidlertid nødvenlig for å oppnå nøyaktige, reproduserbare resultater.

This page was left blank intentionally

Contents

This page was left blank intentionally

1 Introduction

While 71 percent of the Earth's surface is covered by ocean, only around 3 percent of food comes from the sea (FAO, 2022). Fishing has been a source of food for as long as humans walk the Earth, but only in recent years has aquaculture – the farming of fish and other marine life – gained as much traction. The sustainable growth of the aquaculture sector is a great opportunity to secure healthy food for many in a world with a growing population. Ensuring that this is done in a sustainable manner requires strict rules and regulations, which benefit from extensive testing of new designs and production procedures.

Section 1.1 provides background information on the aquaculture sector, fish farm design, and farm locations. Section 1.2 explains the motivation for the research topic and puts it into perspective with current rules and regulations. Section 1.3 lists the objectives, details the scope, and provides expected results of the research.

1.1 Background

The global aquaculture industry is in a phase of steady expansion. A review by Naylor et al. (2021) has shown that the total aquaculture production has more than tripled in live-weight volume over the past two decades. While the majority of the production consists of plants and freshwater species such as kelp and catfish, farming of saltwater species like salmon has seen similar growth as the rest of the sector.

Figure 1.1 – Typical sea site fish farm (Mowi, n.d.)

Norwegian aquaculture accounts for the largest production of farmed fish per capita globally and has seen the fastest growth among developed countries (Garlock et al., 2020). Norwegian fjords provide shelter from waves and wind and it is common to see a floating farm in almost every fjord. An example of such a farm is shown in Figure 1.1.

Concerns for area use and waste accumulation in fjords have increased in tandem with the growth of the industry. Research by Bannister et al. (2016) concluded that organic waste from farms disperses over large areas of fjord systems. This has an impact on the local ecosystem, of which the long-term effects are not yet fully understood. The concerns regarding fish farming inside fjords have led to different options being explored.

One such option is land-based aquaculture. The biggest benefit of this method is that it is a closed system, which means the environment can be controlled. However, this requires land space and a lot of energy for pumps, as well as advanced systems to filter sea water pumped through the tanks.

Another option is building farms in more exposed locations, where space is plentiful and waste is dispersed over a larger area. In general, the wave loads and flow velocity in exposed areas are larger than in sheltered areas. This has an influence on the behaviour of the fish. Hvas, Folkedal, and Oppedal (2021) researched the behaviour of salmon when exposed to stronger currents. One of the effects they found is that when the current exceeds the swimming capacity of the fish, individuals become fatigued and get pushed to the back of the net. This can cause the build up of substances which influence the quality of the fish.

Furthermore, the growth of the sector has caused an incentive for larger farms and new designs. The Norwegian government launched "development licenses" in 2015, focusing on expansion to open ocean areas and reduced waste from inshore systems. This resulted in over a hundred applications, of which 23 were granted a license (Moe Føre et al., 2022). Almost half of the awarded licenses were for closed farms, which could provide a great combination between a controlled environment and using space in the sea instead of on land.

Together, more exposed locations and new designs cause the motions and loads on the structure to be different than those on farms in sheltered areas with a more mature design. In Figure 1.2, a typical fish farm design is shown exposed to waves.

Figure 1.2 – Fish farm in waves (ScaleAQ, n.d.)

1.2 Motivation

While much of the knowledge and testing procedures stem from experiences in the offshore oil and gas sector, rules and regulations are becoming stricter and more specific to the aquaculture sector. The Norwegian Standard NS9415 describes the rules for new and existing fish farms. A large update to this standard came into effect in the start of 2023 (Fiskeridirektoratet, 2023). In relation to these new rules, creating an experimental setup for testing the wave motion response of fish farms in the model tank at NTNU in Ålesund will provide insights in the environment and limitations at this facility. Measuring the motion response of a fish farm model will show that it is possible to conduct these measurements at a relatively small facility.

1.3 Objectives and scope

The primary objective of the study is to create an experimental setup and measure the wave motion response of a model fish farm.

The primary objective is split as follows:

- Obtain an understanding of the wave characteristics in the model tank at NTNU in Ålesund
- Create a physical and digital model of a fish farm
- Define a test procedure for carrying out wave response experiments
- Design a sensor setup to measure relevant parameters
- Analyse the wave motion response of the model

Chapter 2 details the research on the wave characteristics in the model tank. The focus is on regular waves, using linear and second-order wave theory as a theoretical background. A new system for measuring the water level is set up and regular wave tests are conducted. These tests are conducted for a selection of wave periods that have been used in the past, as well as a selection of wave steepness used in other research on floating structures. The results of these tests are analyzed to obtain the limitations of the model tank. From previous experience, it is expected that shorter waves – with a lower wave period – will be more accurate to their corresponding theoretical wave.

Chapter 3 describes the process of creating the physical and digital model. It also explains the theory used in dynamic response analysis. The physical model of the fish farm is created using widely available materials. The assumed model scale is 1:75, which means the full-scale dimension of the farm would be comparable to existing farms. However, the model is not made to represent any specific design. The fish farm is also modelled in AquaSim, a software specialized in the analysis of flexible structures. The digital simulation is used to obtain the frequency response characteristics of the model to compare with the physical experiment.

Chapter 4 explains the main experiment. The theory used to process the measurements is presented, the experiment plan is explained, and the sensor setup is listed. It is expected that creating the experimental set up will take more time than initially thought, so it was decided to only create one model instead of various farm designs. The position of the model is measured using a motion-tracking camera system. Together with the results from the wave tests, this is used to obtain the frequency response characteristics of the model. It is expected that while each separate measurement might not correspond to the digital simulation, the overall result will be similar.

Chapter 5 brings all the results together and provides the conclusions, limitations and recommendations for further work.

This page was left blank intentionally

2 | Wave environment

Ocean waves influence all sorts of man-made structures at sea. Waves can be generated by a variety of sources, which together create the wave environment a structure is exposed to. Examples of wave sources include tides, wind, and other man-made structures moving in water. An example of ocean waves – in this case caused primarily by wind acting on the water surface – is shown in Figure 2.1. A single expression for the complete wave environment from all sources does not exist; even in simple cases an approximation is required.

In the case of waves in model tanks like the one at NTNU in Ålesund, the water depth can have a significant influence on the wave characteristics. It is also assumed that waves propagate in a single direction – that is, there is no variation in the flow perpendicular to the propagation direction. Another important simplification is the use of regular waves, where the frequency and amplitude of the wave does not change over time.

Section 2.1 provides a comprehensive overview of the wave theory used to describe the environment in the model tank. The theory used in this chapter is adapted from lecture notes on regular wave theory by Karl H. Halse (2021), as well as the books Offshore Hydromechanics (Journée and Massie, 2001) and Linear and Nonlinear Waves (Whitham, 1999). Section 2.2 explains how to classify the wave exposure. Section 2.3 describes the wave test procedure and compares the measured results to the wave theory.

Figure 2.1 – Wind waves breaking near the shore of Runde, Norway

2.1 Wave theory

Linear wave theory is often used to describe the propagation of ocean waves. It uses potential theory, which assumes the fluid is inviscid, irrotational and incompressible. This results in a harmonic function for the wave elevation such as the one shown in Equation (2.1).

$$\zeta(x,t) = \zeta_a \cos\theta \tag{2.1}$$

Figure 2.2 shows a visual representation of such a linear regular wave in two perspectives: 2.2a shows the wave elevation at a single point in time, 2.2b shows the motion of the wave at a given location. Note that the coordinate system is centered around the still water level $z = 0$, with the vertical axis **z** directed upward. The free surface is located at $z = \zeta$ and the seabed is at $z = -h$. These locations are important to remember for later, when working with the boundary conditions of the environment.

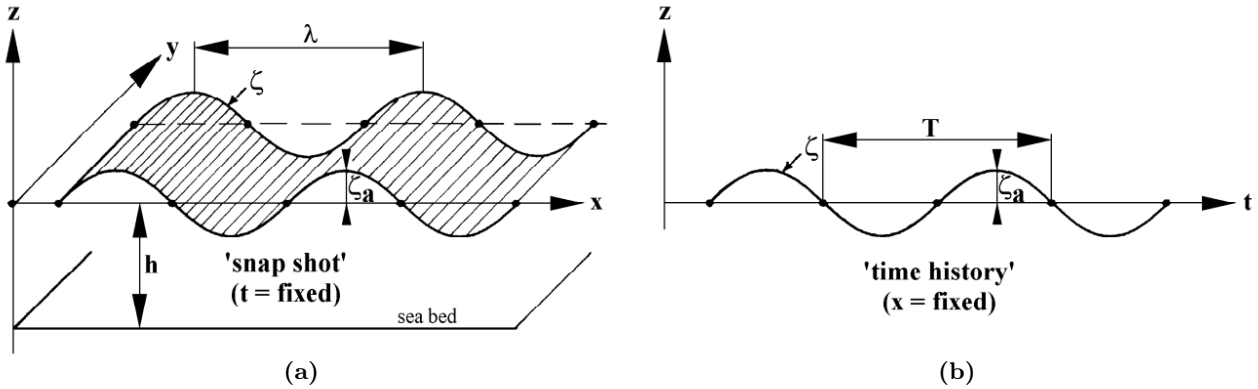

(a) **(b)**

Figure 2.2 – Visual representation of a linear regular wave (Journée and Massie, 2001, p. 5-4).

Figure 2.2a also shows the wave length λ, the distance between two wave peaks. Figure 2.2b shows the wave period T, the time between two wave peaks. Both figures show the wave amplitude ζ_a. Table 2.1 lists these parameters and gives an overview of the other important parameters used to describe regular linear waves.

Table 2.1 – Parameters of regular linear waves

Quantity	Symbol	Unit	Expression
Wave elevation	$\zeta(x,t)$	-	$\zeta = \zeta_a \cos\theta$
Wave phase	$\theta(x,t)$	-	$\theta = kx - \omega t$
Wave length	λ	m	
Wave number	k	m^{-1}	$k = 2\pi/\lambda$
Wave period	T	s	
Angular frequency	ω	s^{-1}	$\omega = 2\pi/T$
Mean water depth	h	m	
Wave amplitude	ζ_a	m	
Wave height	H	m	$H = 2\zeta_a$
Wave steepness	ϵ	-	$\epsilon = H/\lambda$

The wave length and frequency of a water wave cannot be chosen independently. They are related by the dispersion relation, shown in Equation (2.2).

$$\omega^2 = kg \tanh kh \tag{2.2}$$

To relate the wave elevation to other quantities such as pressure and force, the velocity potential $\phi(x, z, t)$ is defined. Using linear theory means that this function has a linear relation with the harmonic wave elevation function. This relation is included in the definition of the velocity potential in Equation (2.3), where $P(z)$ is a yet unknown function dependent on the distance below the still water level.

$$\phi(x, z, t) = P(z) \cdot \sin\, \theta \tag{2.3}$$

The governing equation for the velocity potential is the conservation of mass in the fluid. Given that the fluid is incompressible and the wave propagates in a single direction, this is defined as shown in Equation (2.4).

$$\nabla \vec{\mathbf{U}} = \frac{\partial u}{\partial x} + \frac{\partial w}{\partial z} = 0 \tag{2.4}$$

The velocity of the water particles in the two translational directions follow from the velocity potential as in Equation 2.5.

$$u = \frac{\partial \phi}{\partial x} \quad \text{and} \quad w = \frac{\partial \phi}{\partial z} \tag{2.5}$$

Combining (2.4) and (2.5) results in the Laplace equation, shown in Equation (2.6).

$$\nabla^2 \phi = \frac{\partial^2 \phi}{\partial x^2} + \frac{\partial^2 \phi}{\partial z^2} = 0 \tag{2.6}$$

Substituting the velocity potential (2.3) into (2.6) results in a homogeneous solution for $P(z)$, shown in Equation (2.7).

$$P(z) = C_1 e^{kz} + C_2 e^{-kz} \tag{2.7}$$

To determine the two unknowns, three boundary conditions are identified.

Firstly, the kinematic seabed condition states that there is no flow in vertical direction at the bottom, as the sea bed is considered to be water tight. This condition is also known as the no-leak or no-flux condition, shown in Equation (2.8).

$$\frac{\partial \phi}{\partial z} = 0 \quad \text{at} \quad z = -h \tag{2.8}$$

Secondly, the kinematic free surface condition states that a particle on the water surface must remain on the water surface, shown in Equation (2.9). In linear wave theory, the second term can be neglected such that $\frac{\partial \zeta}{\partial t} = \frac{\partial \phi}{\partial z}$.

$$\frac{\partial \zeta}{\partial t} + \frac{\partial \phi}{\partial x} \cdot \frac{\partial \zeta}{\partial x} - \frac{\partial \phi}{\partial z} = 0 \quad \text{at} \quad z = \zeta \tag{2.9}$$

Finally, the dynamic condition at the free surface states the fluid pressure on the surface must be equal to the atmospheric pressure, shown in Equation (2.10). In linear theory, this can be simplified to $\frac{\partial \phi}{\partial t} = -g\zeta_a$.

$$p - p_a = \frac{\partial \phi}{\partial t} + \frac{1}{2}\left(\frac{\partial \phi}{\partial x} + \frac{\partial \phi}{\partial z}\right)^2 + g\zeta_a = 0 \quad \text{at} \quad z = \zeta \tag{2.10}$$

Solving the Laplace equation involves substituting the boundary conditions into the velocity potential and determining the two unknowns. This process is not explained here, but can be found in a variety of different sources, such as Chapter 5 of Offshore Hydromechanics (Journée and Massie, 2001). The linear solution for the velocity potential that is commonly used is shown in Equation (2.11).

$$\phi(x, z, t) = \frac{\zeta_a g}{\omega} \cdot \frac{\cosh k\,(h + z)}{\cosh kh} \cdot \sin\, \theta \tag{2.11}$$

Linear wave theory can be expanded by a variety of different theories. Doing this becomes more relevant when the water depth decreases or the wave steepness increases, such as near the shore or in model tanks. The wave propagation can then be modelled using the Korteweg-de Vries (KdV) equation, a non-linear partial differential equation whose solutions can be exactly defined. Examples of solutions include the shallow water theory and cnodial waves, for relatively low amplitude and long waves. For higher amplitude, perhaps the simplest expansion is using Stokes theory.

Stokes started by expanding the linear solution using a perturbation series approach to approximate the non-linear solution. This is shown in Equation (2.12), where ζ_1 and ϕ_1 are the linear solutions. The contributions are scaled by the non-dimensional wave steepness ϵ, which is in general a small quantity. This means higher-order contributions become less important.

$$\begin{aligned} \zeta &\approx \epsilon\zeta_1 + \epsilon^2\zeta_2 + \epsilon^3\zeta_3 + ... \\ \phi &\approx \epsilon\phi_1 + \epsilon^2\phi_2 + \epsilon^3\phi_3 + ... \end{aligned} \tag{2.12}$$

By keeping only the linear and second order terms, a second-order Stokes wave is obtained. Solving the wave elevation and velocity potential for arbitrary water depth, such as in model tanks, requires some extensive algebra and is not explained here. One approach can be found in Chapter 13 of Linear and Nonlinear Waves (Whitham, 1999), which presents Stokes' approach on the KdV equation. Figure 2.3 shows the wave elevation of such a second-order Stokes wave. The first harmonic is the linear solution and the second harmonic is an approximation of the non-linear solution, which are added to find the second-order wave elevation.

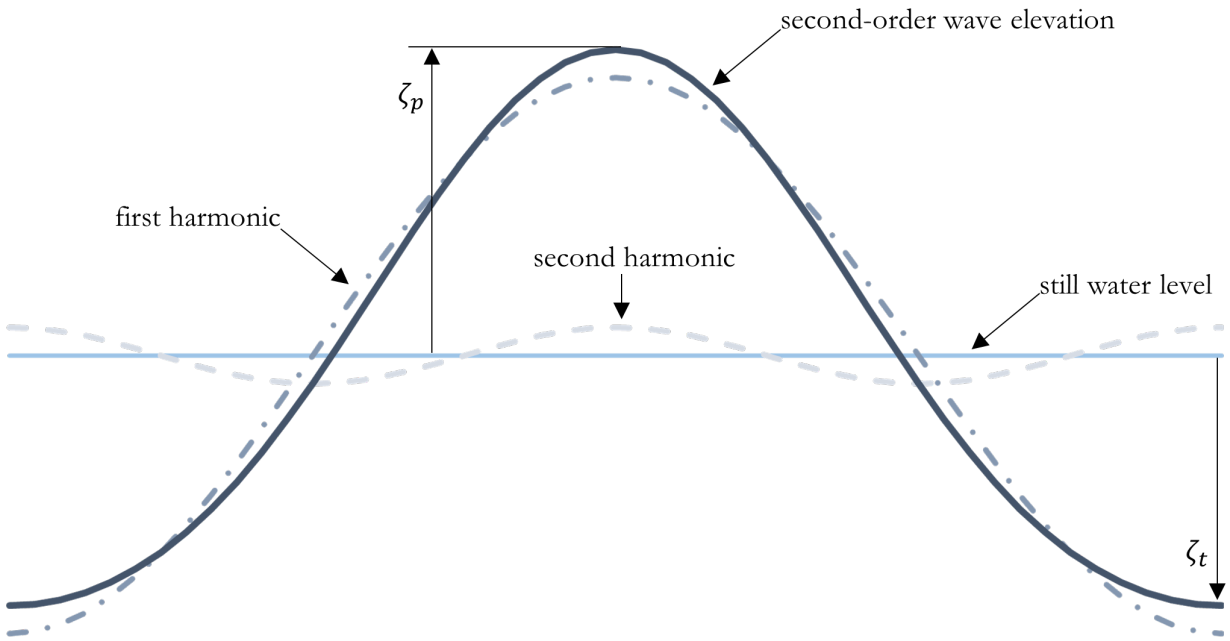

Figure 2.3 – Second order Stokes wave with two contributing harmonics[1]

One of the typical characteristics of waves in limited water depth which Figure 2.3 shows and the Stokes theory captures quite well, is that the waves have steep peaks and flat troughs. The amplitude of the peak is defined as ζ_p and that of the trough as ζ_t. The wave amplitude ζ_a can then be calculated by taking the average of these two.

[1]Figure inspired by Wikipedia on Stokes waves (link). The wave steepness $k\zeta_a$ in this case is equal to 0.2.

The main result of Stokes' research is that the dispersion relation involves the wave amplitude. This is shown in Equation (2.13), where the part in brackets can be seen as an added factor to the linear dispersion relation (Eq. 2.2). In practice, this means that waves with a higher amplitude propagate faster than they would as predicted with linear theory.

$$\omega^2 = kg \tanh kh \left(1 + \frac{9 - 10\tanh^2 kh + 9\tanh^4 kh}{8\tanh^4 kh} (k\zeta_a)^2\right) \tag{2.13}$$

The solution for the second-order wave elevation is shown in Equation (2.14). For deep water, the factor of the second-order contribution approaches $\frac{1}{2}k\zeta_a^2$ as $\tanh kh \to 1$.

$$\zeta(x,t) = \zeta_a \cos\theta + k\zeta_a^2 \frac{3 - \tanh^2 kh}{4\tanh^4 kh} \cos 2\theta \tag{2.14}$$

The second-order velocity potential is shown in Equation (2.15). Note that this includes a drift in time, independent of the position. This drift in the velocity potential causes a reduction in energy as the wave propagates, which in practice contributes to the 'dying out' of waves as they get further from their source. For deep water, both this time drift and the second-order contribution vanish as $\sinh kh \to \infty$.

$$\phi(x,z,t) = \frac{\zeta_a g}{\omega} \frac{\cosh k(z+h)}{\cosh kh} \sin\theta + \frac{3\zeta_a^2 \omega}{8} \frac{\cosh 2k(z+h)}{\sinh^4 kh} \sin 2\theta - (k\zeta_a)^2 \frac{g}{k} \frac{1}{2\sinh 2kh} t \tag{2.15}$$

While the ocean can be seen as infinitely wide and deep in most places, a model tank is far from that. Effects from the walls and bottom of the tank, such as reflection and wave breaking, should be included in the wave theory to obtain an accurate representation of the environment. However, as these effects only cause small variations, the theory used in this research is limited to second-order Stokes waves.

In reality, the ocean does not only contain regular waves and often looks quite 'confused'. Both the wave length, period, and direction are different for every wave. This effect can be captured in a wave spectrum, which is often approximated as the sum of a select number of regular wave components. From this spectrum, two important parameters are found. The significant wave height H_s can be found as the average wave height of the highest 1/3 of the waves in the spectrum. The peak period T_p is the period corresponding the peak of the spectrum. The combination of these two parameters is used to classify the expected wave exposure of a structure in the sea.

2.2 Wave exposure

The classification of wave exposure is defined in Norwegian Standard NS9415, which details requirements for site survey, risk analyses, design, dimensioning, production, installation and operation of marine fish farms (Standard Norge, 2009; Standard Norge, 2021). Table 2.2 shows the classification based on the significant wave height and peak period.

Table 2.2 – Wave classification (Standard Norge, 2009, p. 73)

Class	H_s (m)	T_p (s)	Designation
A	0.0 - 0.5	0.0 - 2.0	Little exposure
B	0.5 - 1.0	1.6 - 3.2	Moderate exposure
C	1.0 - 2.0	2.5 - 5.1	Substantial exposure
D	2.0 - 3.0	4.0 - 6.7	High exposure
E	> 3.0	5.3 - 18	Extreme exposure

NS9415 states that when regular waves are used for testing, the wave height should be equal to 1.9 H_s. This is a conservative estimate of the maximum wave height a farm might be exposed to during a 3 hour storm, where H_s is the significant wave height experienced during this storm. The wave period should be taken equal to the peak period T_p of the spectrum. In selecting a location for a new farm, these estimations give the harshest wave environment the farm will realistically be exposed to.

2.3 Wave tests

The wave tank at NTNU in Ålesund is 10 meters long, 2 meters wide, and has a mean water depth of 85 centimeters. Regular waves and wave spectra can be generated using a single-flap wave maker on one end of the tank. The waves are damped by a parabolic beach at the other end of the tank. A diagram of the tank is shown in Figure 2.4.

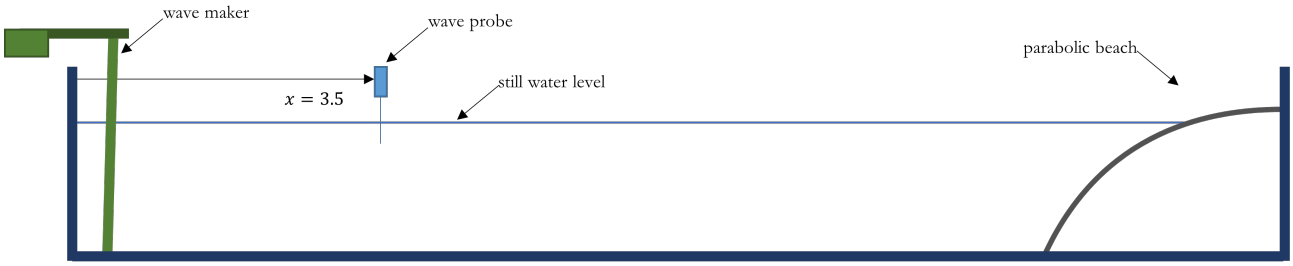

Figure 2.4 – Towing tank at NTNU in Ålesund

From previous experience, the range of periods that the wave maker can create is between 0.5 seconds and 2 seconds. In other studies, steepness values ϵ range between 1/120 and 1/30 (Mukhlas et al., 2021; Faltinsen and Shen, 2018). $\epsilon = 1/15$ was also included in the tests to capture some more extreme waves.

Table 2.3 shows the theoretical wave height given as input to the wave maker. The wavelength λ is calculated from the period T with the linear dispersion relation (see Table 2.1 and Equation (2.2)). The wave height is then $H = \epsilon \cdot \lambda$.

Waves that are impossible to make in this tank, because of a too low or too high amplitude, are blacked out. The other colours indicate the wave classification, corresponding to the colours in Table 2.2. Classification of the waves is done by scaling the regular wave height with the assumed model scale of 1:75 and dividing by 1.9 to obtain the corresponding H_s value. The period is not taken into account in the classification, as most of the periods defined in the regulations are impossible to make in this tank. The classification should thus be seen as a crude indication of the wave exposure.

Table 2.3 – Test waves

T (s)	λ (m)	Wave height H (mm)					
		$\epsilon = 1/120$	1/90	1/60	1/45	1/30	1/15
0.5	0.39	3.3	4.4	6.5	8.7	13.1	26.2
0.8	0.96	8.1	10.7	16.1	21.5	32.2	64.4
1.1	1.80	15.0	19.9	29.9	39.9	59.8	119.7
1.4	2.86	23.8	31.7	47.6	63.5	95.2	190.4
1.7	3.93	32.7	43.6	65.4	87.3	130.9	261.8
2.0	4.83	40.3	53.7	80.6	107.4	161.1	322.2

The combinations in Table 2.3 were given as input to the wave maker. The wave probe was placed at $x = 3.5$m from the side of the wave maker. For more information about the wave probe and its calibration, see Section 4.3. The analysis in this research is limited to the amplitude of the waves. To find the amplitude, the start-up and dying out of the time series is first filtered out. Then, the local maxima and minima in the data are found. For more information about the signal processing, see Section 4.1. Taking the average of the local maxima and minima results in the peak amplitude ζ_p and trough amplitude ζ_t, which are added together to find the measured wave height Hm.

Figure 2.5 shows a test of 600 periods, around 10 minutes. The top plot shows the time series, while the bottom shows the variation in peak amplitude over time. Dividing the data in equal segments allows the creation of a box plot, showing the mean and variation of the data. The first segment includes the start-up which is not visible in the time series. The other segments show the variation remains similar over the whole time range. Therefore, it was decided that for the wave tests generating 50 periods is sufficient.

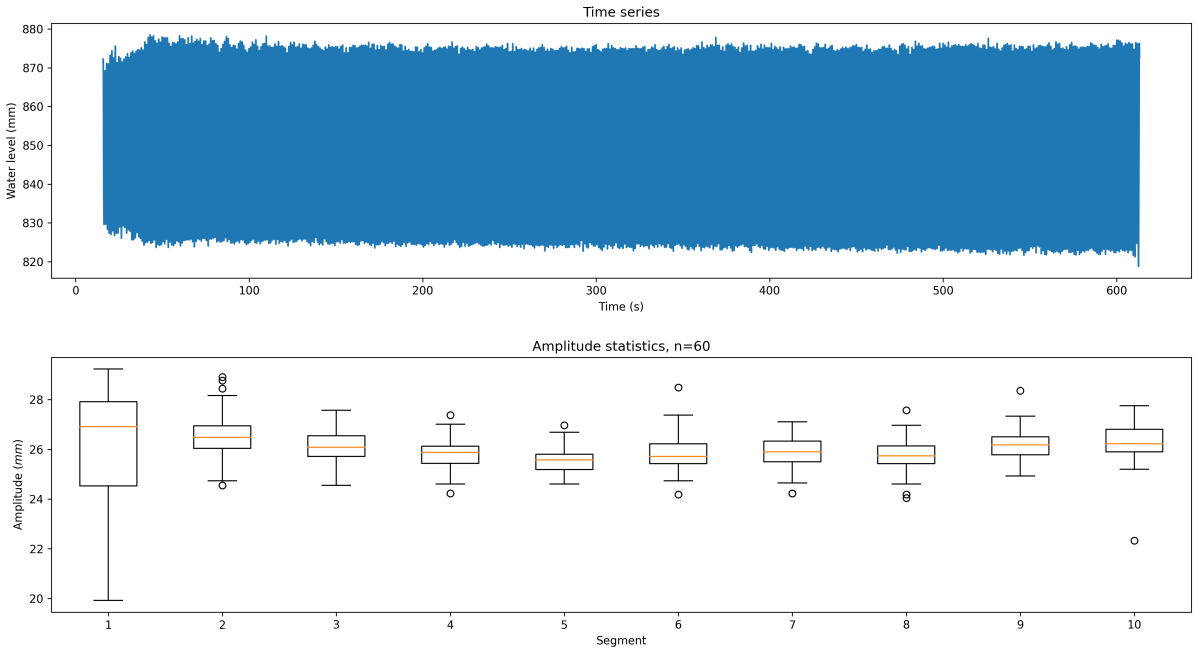

Figure 2.5 – Long-term amplitude variation

2.4 Results

Figure 2.6 shows the time series of two selected waves: 2.6a shows a wave with a low steepness, $T = 1.7$s and $\epsilon = 1/120$. 2.6b shows a wave with a high steepness, $T = 0.8$s and $\epsilon = 1/15$. The dying out of the wave was not further examined, but could be analyzed to find information on the reflections from the wave beach.

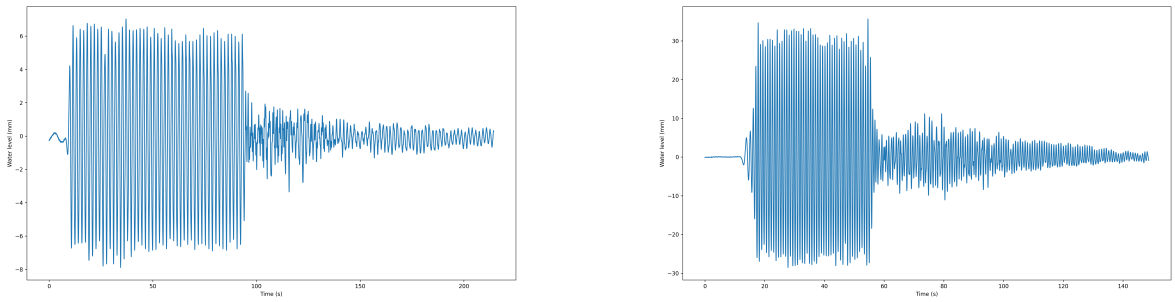

(a) Low steepness **(b)** High steepness

Figure 2.6 – Time series

Figure 2.7 shows the filtered time series – without start-up and dying out – for the same waves. The variation in amplitude in both graphs is representative for the variation found in all tested waves, and this effect is independent of the wave period. It is expected the variation is caused by the control of motion of the wave maker, however this was not further researched and the average values of the amplitude were assumed to be of a sufficient accuracy.

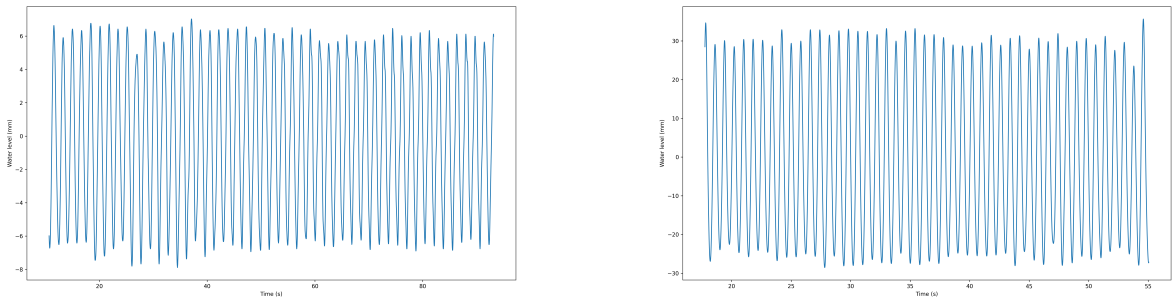

(a) Low steepness **(b)** High steepness

Figure 2.7 – Steady part of the time series

Figure 2.8 shows a steady part of both waves. A least-squares fit of a linear and second-order wave is applied, which follow respectively Equation (2.1) and (2.14). This process shows the importance of the second-order wave theory when the wave steepness is large. In 2.8a, both theories fit the measurement equally well, while in 2.8b the linear theory fails to capture the peaks and troughs. The second-order wave follows the measurement better, even though there are some small dissimilarities, particularly in the troughs. While it is suspected that these are caused by a different non-linear effect, and/or reflected waves, this was not further researched.

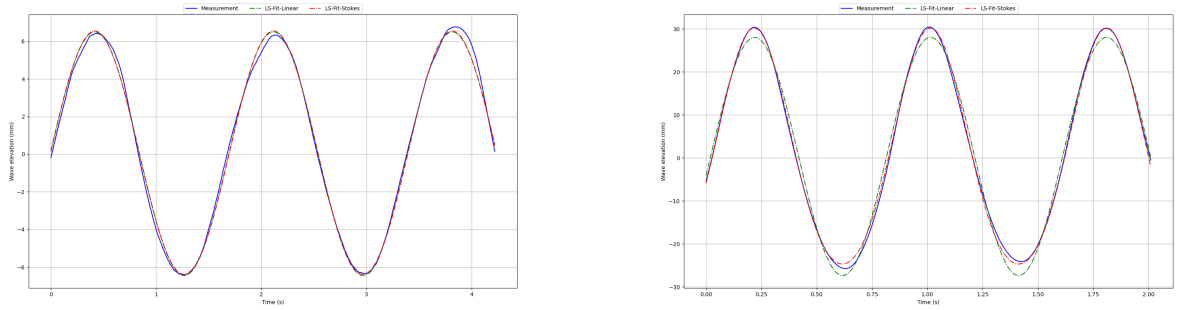

(a) Low steepness **(b)** High steepness

Figure 2.8 – Least-squares fit of theoretical waves

Combining the resulting wave height of every test provides an overview of the wave environment in the tank. Figure 2.9 shows the comparison of the theoretical wave height (solid lines) to the resulting measured wave height (points). The theoretical wave height is calculated using the same method as the values in Table 2.3, by determining the wave length with the linear dispersion relation and calculating the wave height with the wave steepness.

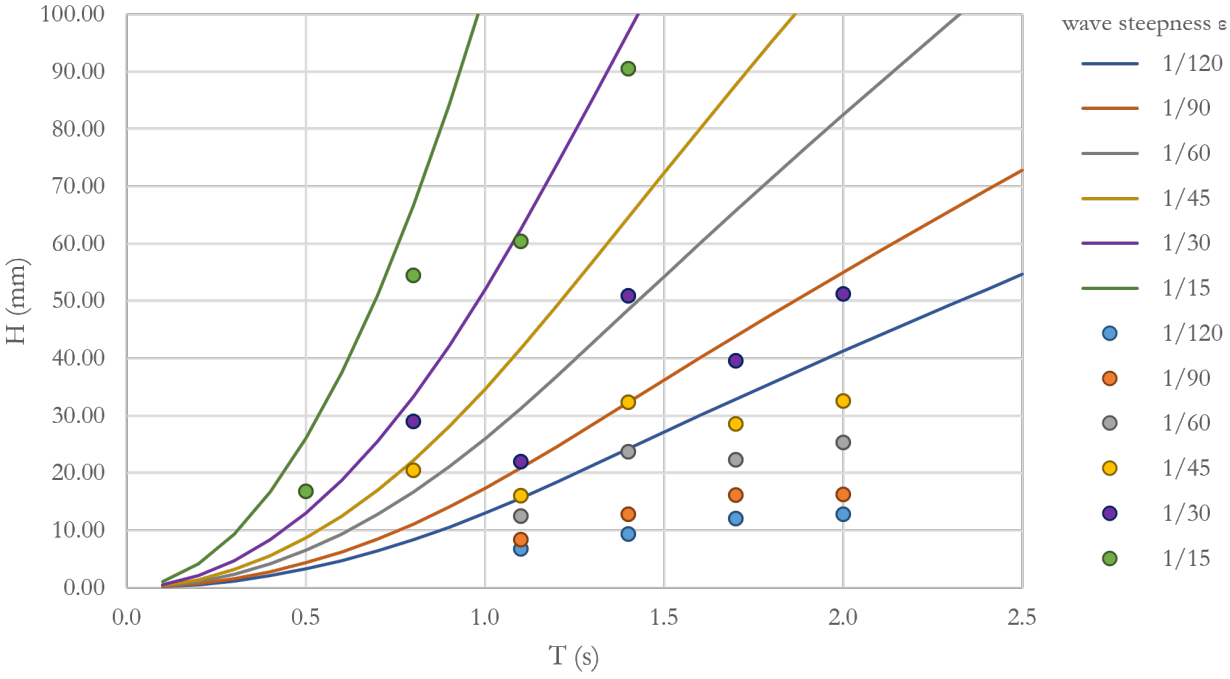

Figure 2.9 – Comparison of theoretical to measured wave height

Figure 2.10 shows the ratio of measured to theoretical wave height – that is, how close the waves get to their theoretical value. The graph shows there is not a large spread in the data points for a single wave period, which implies that the limitations in wave height are more related to the wave period itself rather than the wave steepness. It appears that there is an optimum at a period of 0.8s, as the measured values here approach the theoretical wave height.

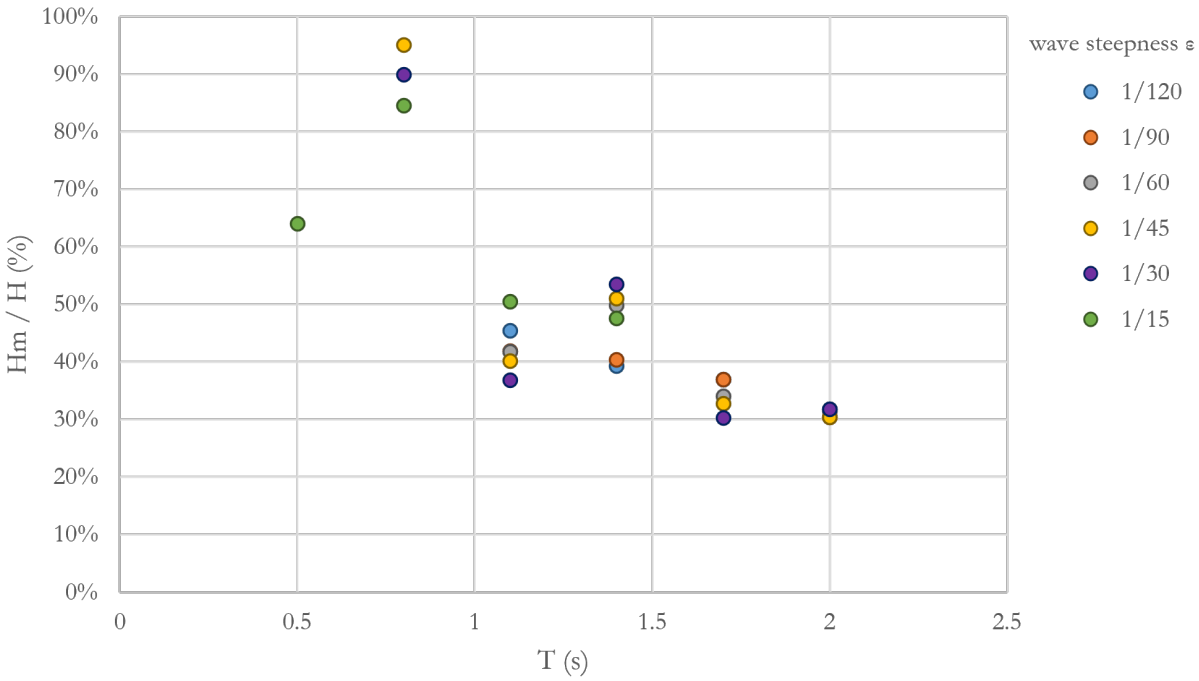

Figure 2.10 – Comparison of input to measured wave height

3 | Response modelling

The motion response of a floating structure is primarily influenced by the waves the structure is exposed to. The wave cause motions and forces on the structure, both directly and indirectly. Performing model tests is often done to predict the motion response of the structure over the range of frequencies it might expect to encounter. Digital simulations are used with the same goal.

The model in this research consists of a fabric net, floater, and mooring system. The model scale is based on the diameter of the model compared to industry standard and is assumed to be 1:75. A physical model is made from widely available materials and a digital model is made in AquaSim, a software which is specialized in solving the motion response of flexible structures. A diagram of the model is shown in Figure 3.1.

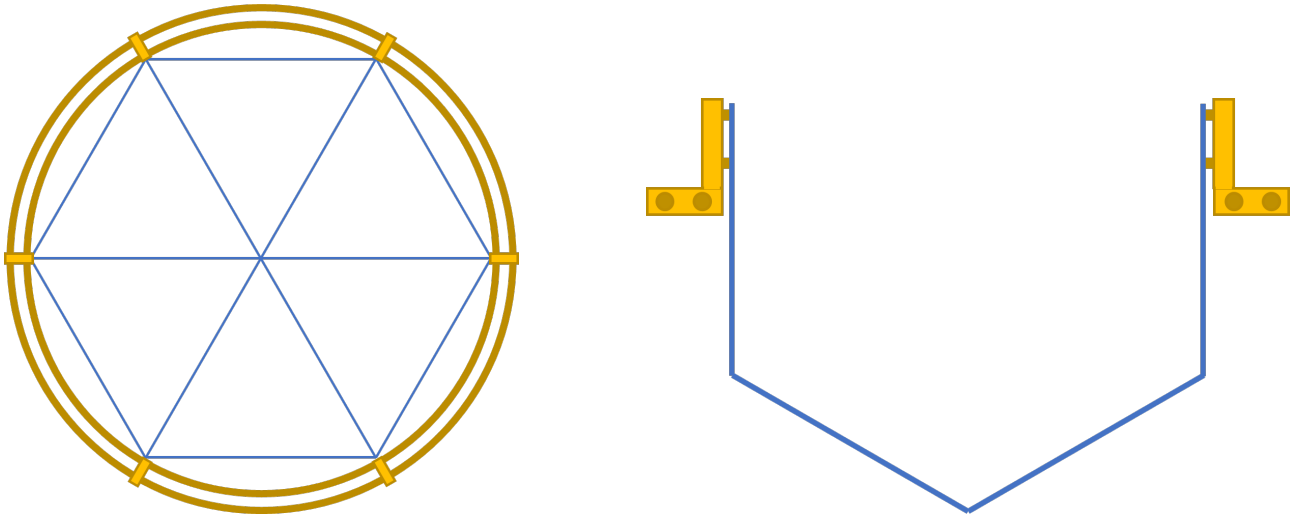

(a) Top view **(b)** Side view

Figure 3.1 – Model diagram

Section 3.1 provides a theoretical background on response analysis. Section 3.2 describes the creation of the physical model. Section 3.3 describes the digital modelling process.

3.1 Response of floating structures

In the motion analysis of floating structures, the Response Amplitude Operator (RAO) is often used. This is effectively a transfer function, relating the motion of the structure to the excitation by the environment – e.g. the incoming wave. For ships and other floating structures, the motion is considered to be linear. The Newton equation of motion of such a system is shown in Equation (3.1), for a single rigid body motion x.

$$[M + A(\omega)]\,\ddot{x} + B(\omega)\dot{x} + Cx = F(\omega) \tag{3.1}$$

Here, the terms on the left hand side represent body forces, while the term on the right represents the excitation force. $[M + A(\omega)]$ stands for the combination of structural mass and added mass, $B(\omega)$ stands for the linear damping, and C stands for the spring term. The force $F(\omega)$ is the harmonic excitation force, which consists of the Froude-Krylov force and diffraction forces. Solving the equation of motion involves inserting the wave elevation ζ into the equation. This process is not explained here, but is described in sources such Offshore Hydromechanics (Journée and Massie, 2001) and Sea Loads on Ships and Offshore Structures (Faltinsen, 1990).

Solving the equation of motion results in graphs such as Figure 3.2, which shows an example of the response characteristics of a floating cylinder. The graph shows three areas, centered around the natural frequency of the object. The low frequency area to the left of the graph is dominated by spring forces, which means the object tends to follow the waves. In the central part of the graph, the motion is amplified by the resonance effect. Here, the motion is dominated by damping, which limits the effect of resonance. Finally, the right part of the graph is dominated by the mass of the object. For higher frequencies, the object is less affected by the waves and will remain mostly stationary.

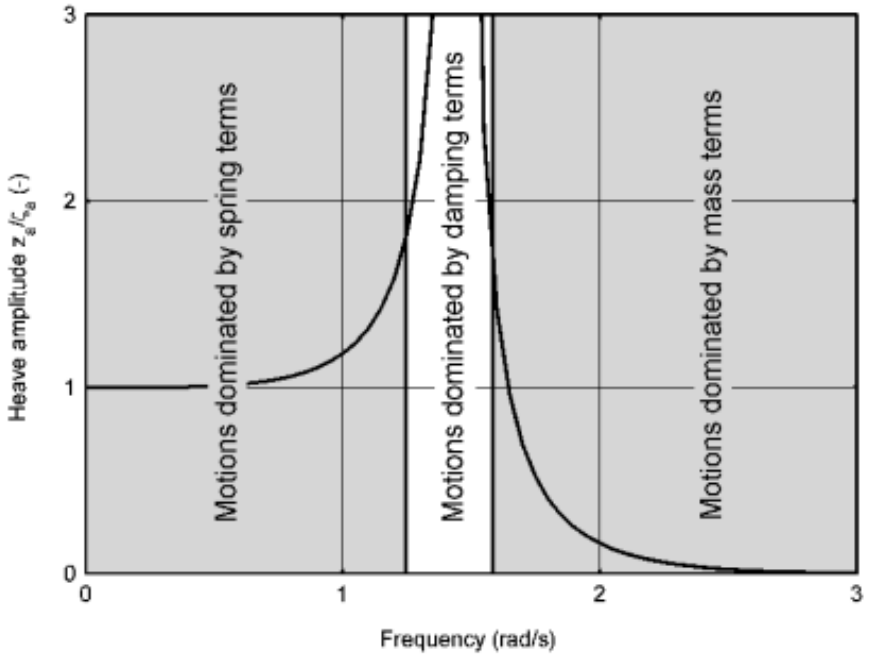

Figure 3.2 – RAO of a floating cylinder (Journée and Massie, 2001, p. 6-24)

An alternative for finding the RAO is measuring the motion response and incoming wave elevation, which is often more practical than attempting to solve the equation of motion. The RAO is then defined as in Equation (3.2), where η is the amplitude of the response and ζ_a is the wave amplitude.

$$RAO = \frac{\eta}{\zeta_a} \tag{3.2}$$

Software such as AquaSim uses Finite Element Analysis to calculate the forces and moments on each part of the structure. This is used to provide a time domain solution of the structural response. A brief description of the methods AquaSim uses to calculate the loads of a structure is given below. More information can be found in the AquaSim Package Theory User Manual (Berstad, 2022).

AquaSim uses three main forms of finite elements:

- Beam elements are 1-dimensional elements that are capable of withstanding load primarily by resisting torsion and axial loads. These are used to model solid structures such as floaters.
- Truss elements are similar to beam elements, except they do not resist bending loads. These elements are primarily used to model ropes and chains.
- Membrane elements are 2-dimensional elements that are used to approximate a net or tarp. They are by definition thin in the normal direction and resist little load in this direction.

AquaSim uses two methods for calculating the excitation forces on the structure. The first is using the Morison equation, which can be seen as a direct method, requiring the hydrodynamic coefficients of the element to be known. An alternative is the second method, Hydrodynamic. This uses strip theory to approximate the loads on the element. Figure 3.3 shows how a floating structure can be subdivided into strips. Each of these strips contains a cross-section of the element, on which the incoming wave potential is solved numerically to calculate the excitation forces on the element.

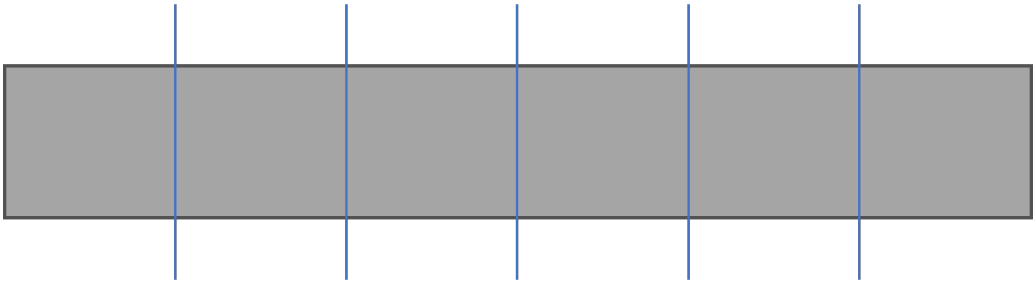

Figure 3.3 – Example of how strip theory is applied to a floating object

3.2 Physical model

The physical model of the fish farm is created using widely available materials. While the assumed model scale of 1:75 means that the model would be representative of existing farms, the model is not made to represent any specific design. Photos of the completed model are shown in Figure 3.4, the properties of the model are summarized in Table 3.1.

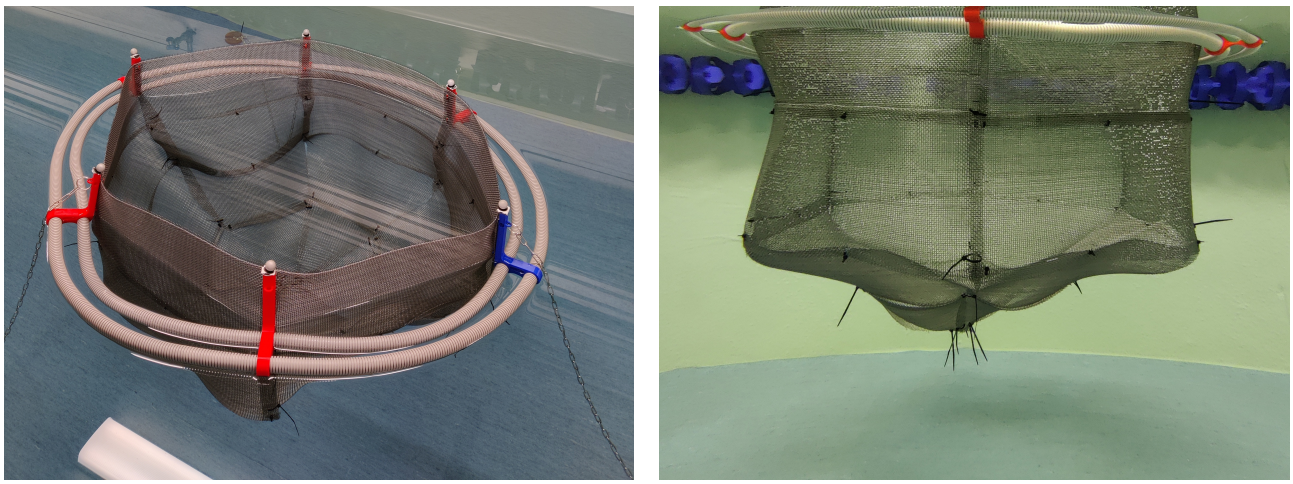

(a) Top view **(b)** Under water

Figure 3.4 – Completed physical model

Table 3.1 – Properties of the model. Full scale values are given for reference

Description	Model scale	Full scale
Floater: polypropylene		
Inner diameter	0.80 m	60 m
Outer diameter	0.88 m	67 m
Pipe diameter	20 mm	1.5 m
Pipe mass	61.5 g/m	26E3 kg/m
Net		
Draught	0.4 m	30 m
Water depth	0.85 m	63.75 m
Mooring system		
Chain length	2 m	150 m
Chain mass	67.0 g/m	28E3 kg/m

The floaters are made of flexible tube conventionally used as electrical conduits, inspired by the typical floatation system seen in existing fish farms and similar to those used in research by Mukhlas et al. (2021). A photo of the tube is shown in Figure 3.5. The flexibility of these tubes was not measured or calculated. However, as there is a large variation in the flexibility of commercial floaters, the tubes are considered to be representative for typical floaters. The tubes are made from polypropelene, a plastic compound with a low density, making it suitable for modelling floating structures.

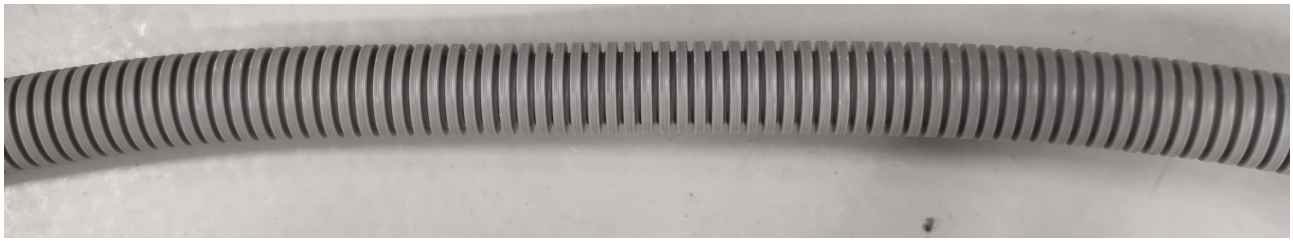

Figure 3.5 – Flexible tube used for the floater

The floaters are held together using six 3D-printed brackets distributed along the circumference. A photo is shown in Figure 3.6. Conventionally, the connectors are made from steel because it is widely available and has a high stiffness. In model scale however, steel brackets would be too heavy and challenging to model. The material used in 3D-printing is PLA, which is a bioplastic with a low melting point, but high strength. This material is considered stiff enough for the brackets' purpose.

The brackets also each feature two 'hooks' used to connect the net, as well as a ring to attach the mooring chain. This ring is located on top of the bracket, because when the brackets were made there was still an idea to measure the force in the mooring lines using load cells. These load cells cannot be under water, which is why the attachment point was lifted up to fit the load cells. In reality, the mooring system would be attached to the outer floater, on the far left in Figure 3.6.

Figure 3.6 – 3D-printed bracket

The net is made out of mosquito netting tied together using zip-ties. A photo of a piece of the net is shown in Figure 3.7. This option was chosen to have a cheap and accessible way to model a net that looks like those used in actual fish farms. The stiffness and hydrodynamic properties of the net have not been researched and it is made of an unknown material. While it is expected that the net will be more stiff than compared to full-scale farms, which influence this will have on the motion of the model was not examined further.

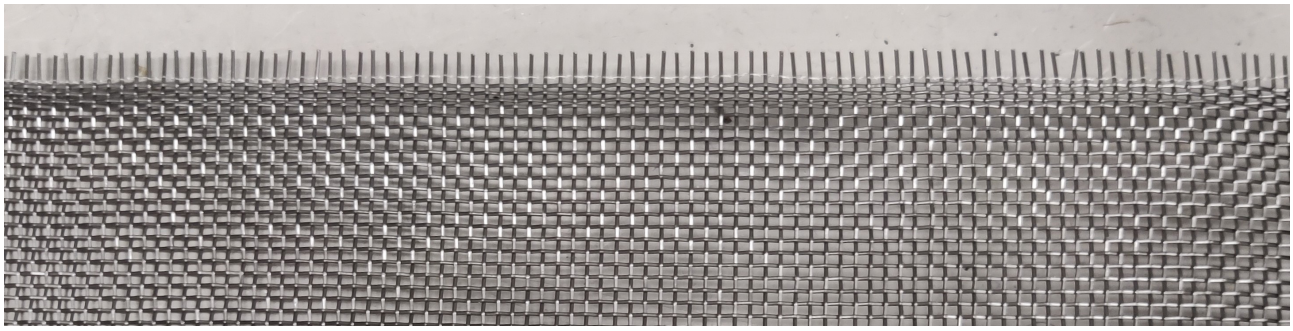

Figure 3.7 – Netting material

The mooring system uses corrosion-resistant chain and weights functioning as an anchor. A photo of the anchor and part of the chain is shown in Figure 3.8. The purpose of the chain and anchor is keeping the model in place. While conventional fish farms use a small piece of chain near the anchor and rope for the rest of the mooring system, it was chosen to only use a chain in this research for simplicity. While it is expected that this influences the motion response of the farm, this effect was not researched further.

Figure 3.8 – Anchor with chain

3.3 Digital model

The digital model is created in the same scale as the physical model. This is done using the 3D-modelling tool included in the AquaSim package, AquaEdit. The finished model is shown in Figure 3.9. The environmental conditions are also set up in AquaEdit. Regular waves are used with a period range of [0.3, 2.5] seconds. The wave amplitude is 0.1 meter for every simulation.

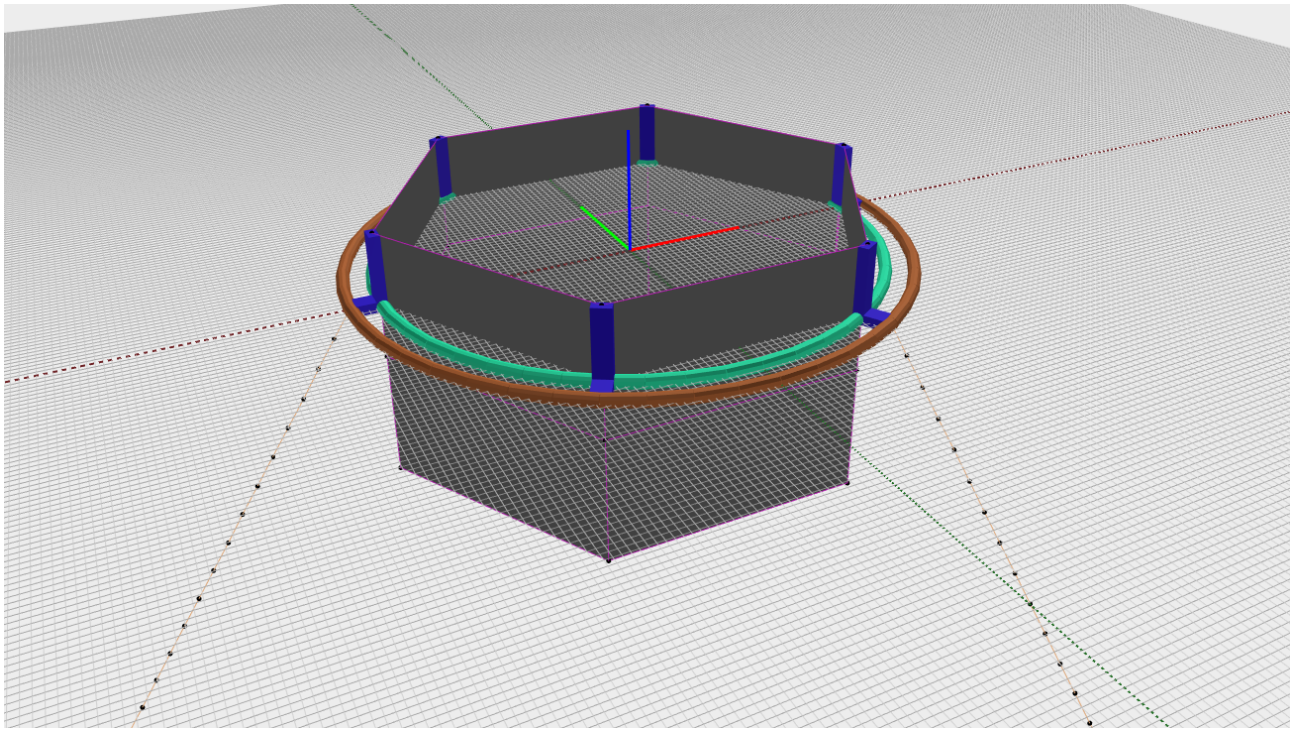

Figure 3.9 – Complete digital model in AquaEdit

The floaters are modelled using beam elements, of which the properties are shown in Table 3.2. In the physical model, the floaters are made of polypropelene. There exists a large range of E- and G-modulus for this material. Combined with the fact that the geometry cannot be modelled exactly, it was chosen to use the default floater material in AquaSim, PE100.

Table 3.2 – Floater properties

Shape: Tube	
Diameter	20 mm
Thickness	3 mm
Material: PE100	
Density	958 kg/m^3
E-modulus	1.0E9 N/m^2
G-modulus	3.8E8 N/m^2
Filled with: Air	

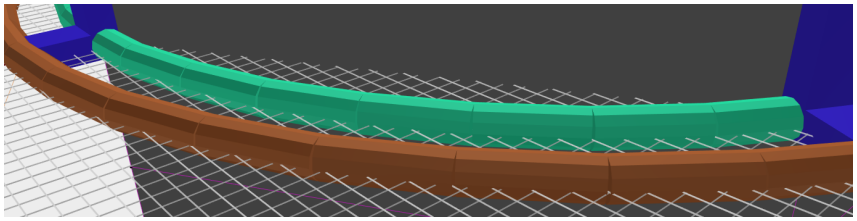

Figure 3.10 – Floaters in AquaSim

The connecting brackets are also modelled using beam elements. The geometry is approximated by a solid rectangular beam, whose dimensions are the same as in the physical model. The brackets are made from PLA, of which the material properties were found in the MatWeb materials database (MatWeb, n.d.). The properties of the brackets are shown in Table 3.3.

Table 3.3 – Bracket properties

Shape: Solid rectangular	
Height	16 mm
Width	28 mm
Material: PLA	
Density	1210 kg/m^3
E-modulus	3.5E9 N/m^2
G-modulus	2.4E9 N/m^2

The net is modelled using membrane elements. Because the net in the physical model has an unknown material and density, its parameters are left standard.

Table 3.4 – Net properties

Thread diameter	2 mm
Density	1025 kg/m^3
E-modulus	1.0E9 N/m^2

The mooring system is modelled using truss elements. The cross-sectional area was estimated as an oval of the same size as the chain links of the physical model. The E-modulus is taken as the typical value for steel, while the weight was calculated by weighing the chain used in the pysical model and dividing by its length.

Table 3.5 – Chain properties

Area	6.28E-6 m^2
E-modulus	2.1E11 N/m^2
Weight	0.067 kg/m

3.4 Results

Aquasim does not have a built-in function for retrieving the RAO of the model. The amplitude of the motion response had to be manually extracted from the time-domain simulation and no time series plots were made. However, the simulation converged for every wave period. The RAO in vertical direction is calculated using (3.2), and shown in Figure 3.11.

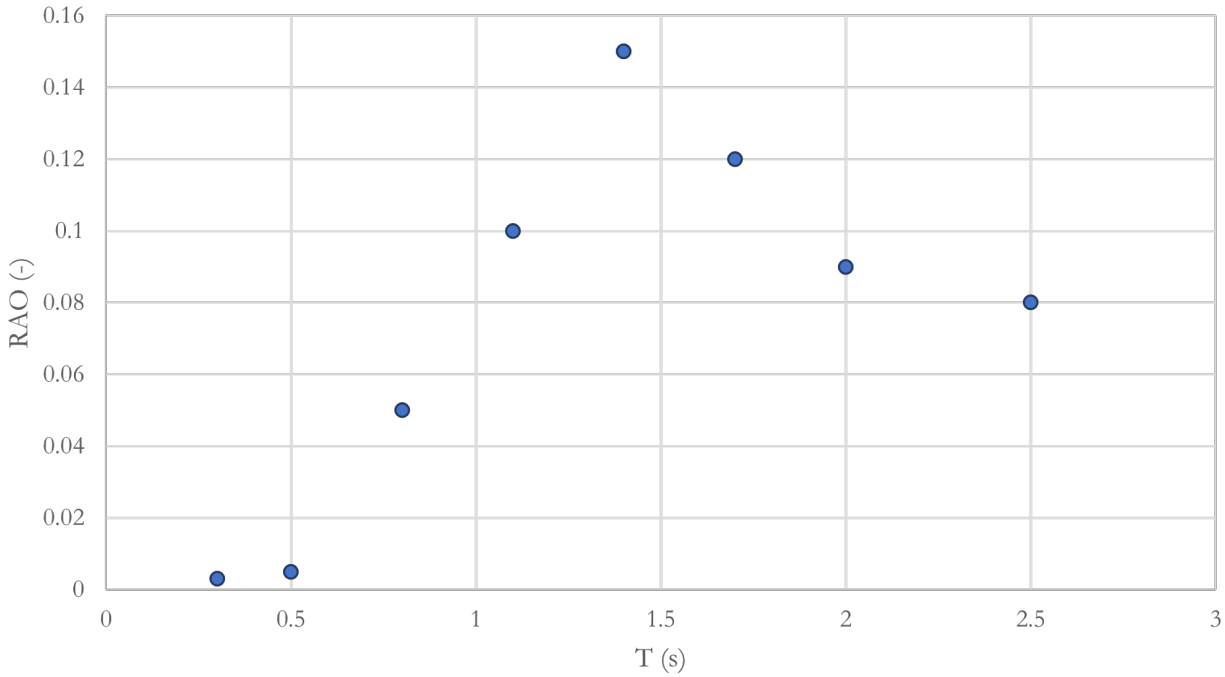

Figure 3.11 – RAO from aquasim

This page was left blank intentionally

4 Response experiment

Experiments are used to test a hypothesis by varying specific parameters that are identified to influence the result. The reason for doing experiments can vary greatly, but in the case of model tank experiments the goal is often to test a design before it is implemented in real scale.

Figure 4.1 shows a diagram of the experimental setup. Note that this diagram is not to scale, in reality the tank is longer.

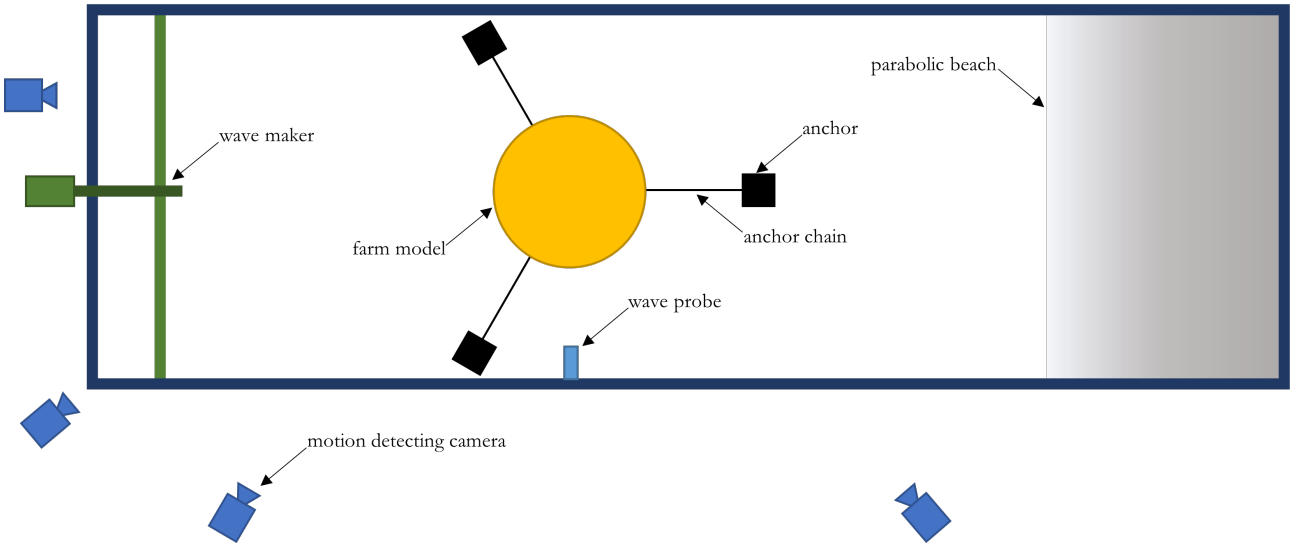

Figure 4.1 – Experimental setup

Section 4.1 provides insight into the methods used to process the data obtained in the experiments. Section 4.2 explains the testing procedure. Section 4.3 lists the sensors and their specifications.

4.1 Signal processing

When a signal is obtained from a sensor, it often contains noise – unwanted disturbances – which needs to be filtered out. Signal noise can be generated by a variety of sources, such as vibrations. Filtering noise can be done to analog signals, using electronic components tuned to the frequency of the signal. Perhaps more common in modern times is using digital filters, which can also be used to smooth the data. An example is using a Savitsky-Golay (`savgol`) filter, a form of moving average.

To find the local maxima and minima of the measurements, an algorithm provided by Henry Piehl is used. This first uses the `savgol` filter to smooth the data, after which it finds the data points at which the curve switches direction. Where the neighbouring points are lower this indicates a local maximum. Conversely, where the neighbouring points are higher this indicates a local minimum.

4.2 Experiment plan

To obtain the motion response of the model, one wave is chosen for every period. Each test is repeated three times to account for variations in the experiment conditions. Table 4.1 shows the waves used in the experiment.

Table 4.1 – Test waves used in the experiment

T (s)	λ (m)	H (mm)
0.5	0.39	26.2
0.8	0.96	32.2
1.1	1.80	39.9
1.4	2.86	47.6
1.7	3.93	43.6
2.0	4.83	40.3

Because the measurements are obtained from two different systems, it is important to know which files correspond to which measurement. The file names are set up to include information about the test. For example, `H047T14.csv` refers to the measurement with $H = 47$ mm and $T = 1.4$ s. The data is stored on the respective devices and transferred to the user PC using a USB drive.

4.3 Sensors

Wave height sensor

The wave height is measured using the system shown in Figure 4.2. A larger picture of the wave probe is shown in Figure 4.3. This consists of two wires, sticking through the water surface. There is a linear relation between the water level and the impedance through the wires, which is measured using a signal created by the WAMP 4000+. This device, designed by Sintef Ocean, creates a signal with a range of [-10, 10] volts, using a carrier frequency to prevent electrolysis of the water. To convert the analog signal to a digital one, the HBM MX840A analog to digital converter is used. In this case, the input range of the device is [0, 10] volts. The digital data is transmitted to the PC using an Ethernet connection. The software on the PC is used to set up the channel information and sampling rate.

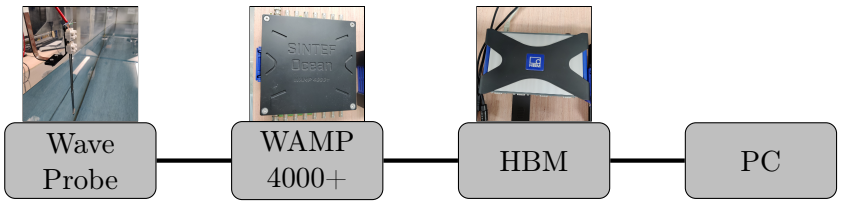

Figure 4.2 – Wave height sensor setup

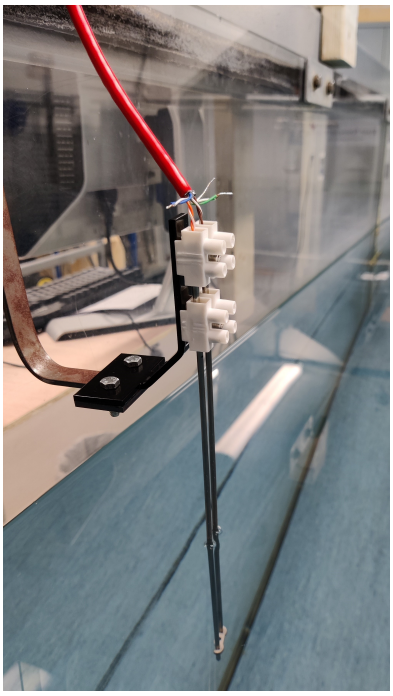

Figure 4.3 – Wave probe

Calibration of the wave height sensor

The voltage signal generated by the WAMP 4000+ is calibrated using the included WPCAL 2000+ device, shown in Figure 4.4. The gain and offset of the signal can be adjusted and the output voltage is shown on the screen. Figure 4.5 shows the calibration setup. The bracket that the wave probe is mounted on can be moved up and down to three positions. First, the wave probe is moved to position C, where the water level is at the lowest. Here, the aim is to adjust the offset so that the output is on the lower end of the range of the analog to digital converter, i.e. 2.5 volts. Subsequently, the wave probe is moved to position B, where the middle of the wires are approximately at the still water level. At this point, the aim is to set the voltage to the middle of the output range, 5 volts. Voltage measurements from points A, B, and C can now be used to calibrate the wave tests.

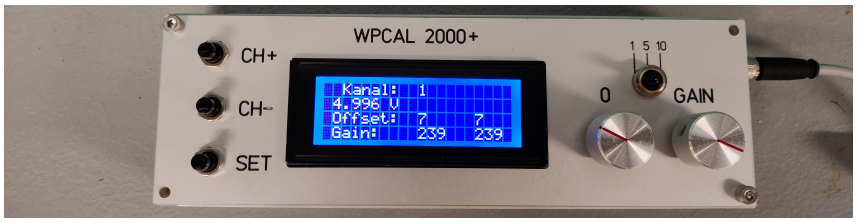

Figure 4.4 – WPCAL 2000+

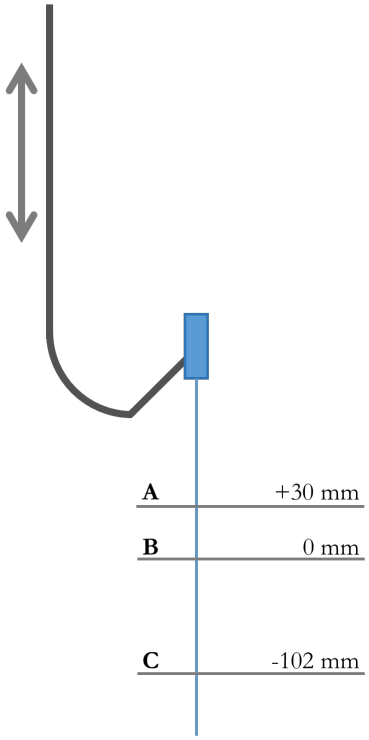

Figure 4.5 – Wave calibration

There is a linear relation between the measured voltage and the water level. When calibrating, first the still water level is measured with a scale installed on the inside of the tank. This is the zero level at position B in Figure 4.5. Then, measurements with a duration of 1 minute are performed at the three locations. The average values of these measurements are used to fit a line, which is used to convert the voltage signal to the water level. An example of the result is shown in Figure 4.6.

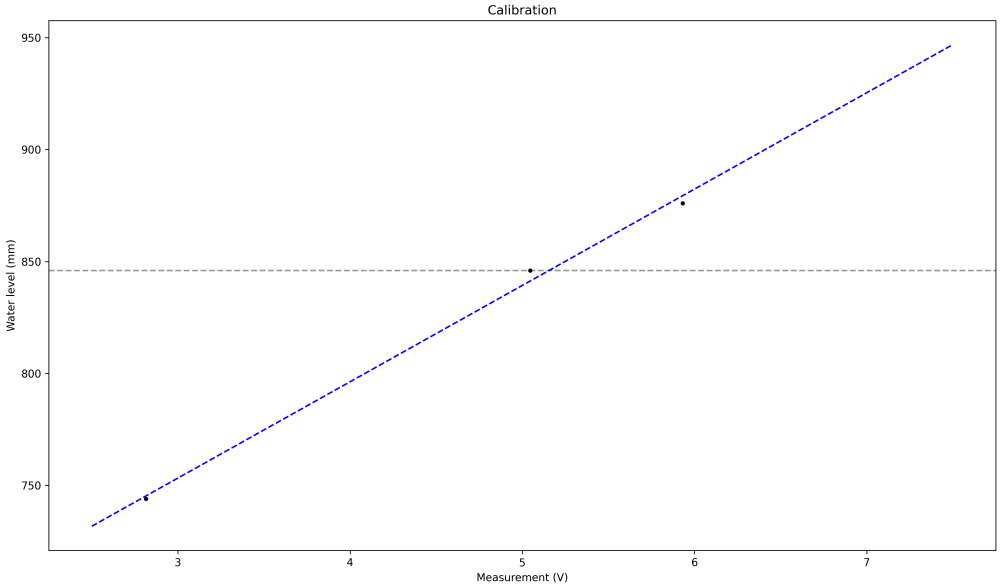

Figure 4.6 – Calibration of the wave height sensor

Motion tracking system

Motion tracking is done with a Qualisys system. This is connected as shown in Figure 4.7. The camera system consists of three Arqus cameras and one Miqus camera. The Arqus cameras use infrared light to determine the distance to specifically designed markers, placed on the model. One of the cameras is shown in Figure 4.8. The Miqus camera takes a video of every measurement, which can be used to overlay data on.

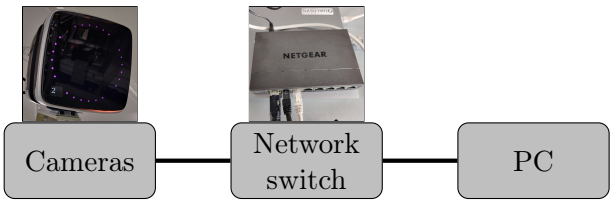

Figure 4.7 – Motion tracking setup

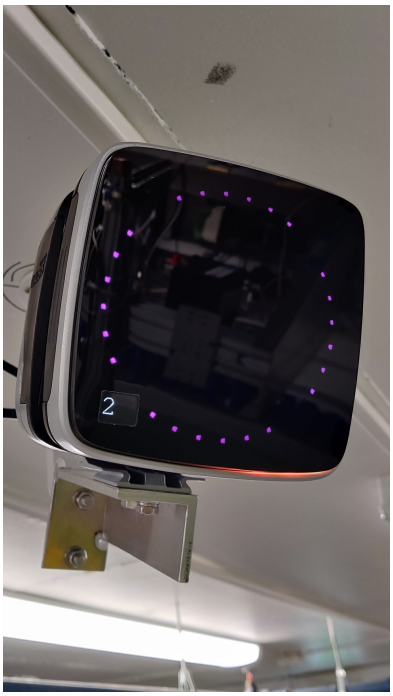

Figure 4.8 – Motion tracking Arqus camera

Calibration of the motion tracking system

The motion tracking system is calibrated using a procedure described in the Qualisys user manual (Qualisys AB, 2022, p. 137). This defines the origin point, which is an L-frame with three markers, shown in Figure 4.9. The origin is placed roughly in the middle of the model tank and is levelled so that it is horizontal. Then, a 'wand'with an additional two markers is moved through the volume covered by the cameras, which enables the system to calculate the distance from each camera to the origin. Later, this is used to calculate the position of the model in relation to the origin.

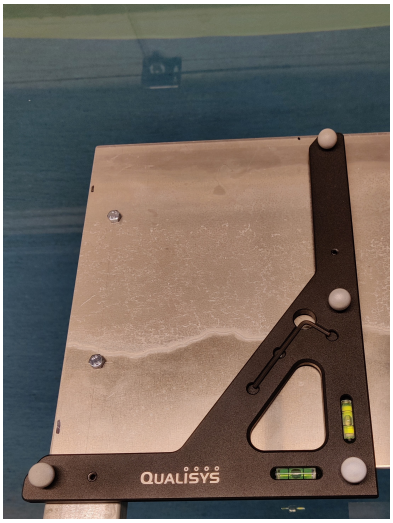

Figure 4.9 – L-frame

4.4 Results

The time series of the vertical position of the model in one of the tests, with $T = 0.8$s, is shown in Figure 4.10. This shows a similar variation in amplitude as in the wave measurements, and also here it is assumed that taking the average to find the amplitude is sufficient for the purpose of this research.

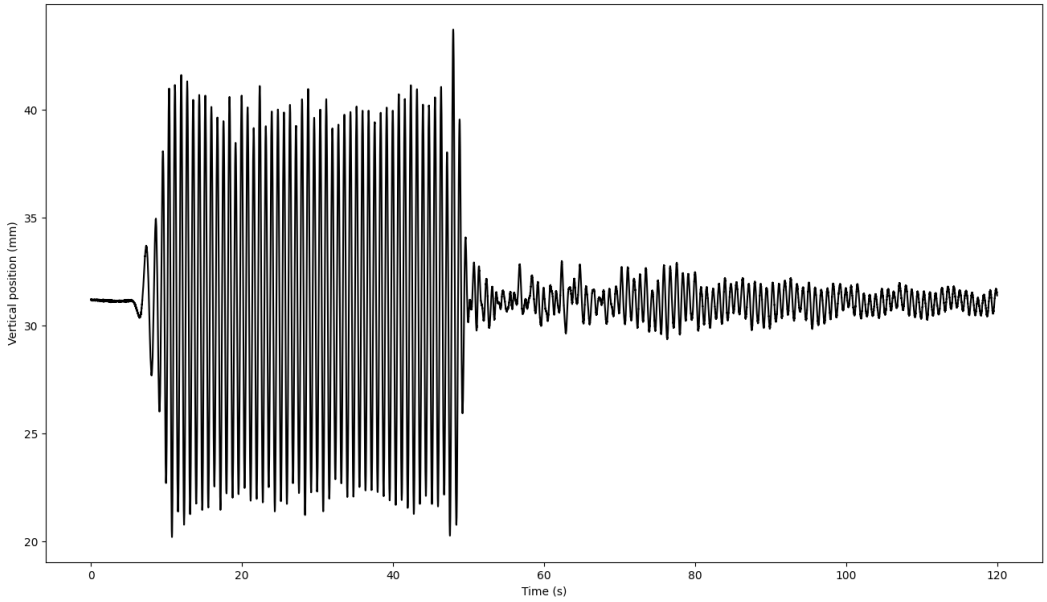

Figure 4.10 – Time series

Equation (3.2) is used to find the RAO in vertical direction for all tests. This results in Figure 4.11.

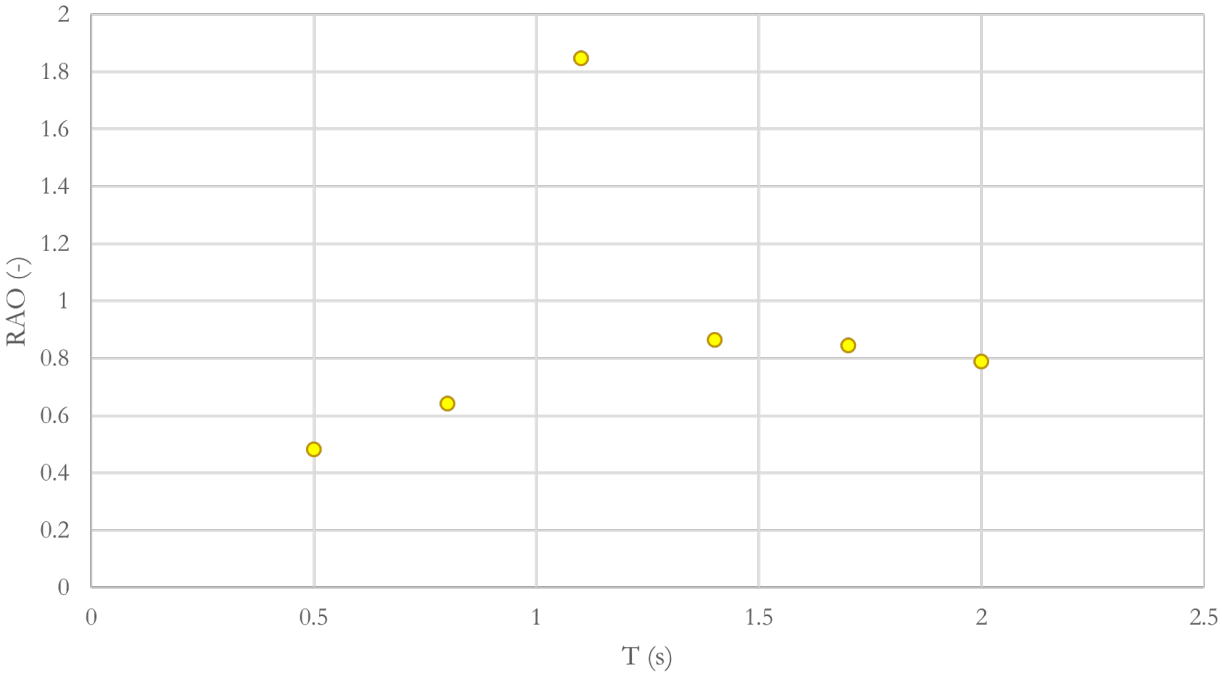

Figure 4.11 – RAO from the model tests

This page was left blank intentionally

5 | Discussion

5.1 Conclusions

From the wave tests, it can be concluded that second-order Stokes theory becomes necessary to include in the theoretical background for the waves when their steepness increases. Furthermore, it became clear that none of the researched waves reach their theoretical wave height. The result is repeated in Figure 5.1. It appears the accuracy of the waves is primarily dependent on the wave period and there is an optimum around $T = 0.8$s. However, more testing – especially for lower periods – is required to confirm or deny the expectation that shorter waves are more accurate in their wave height.

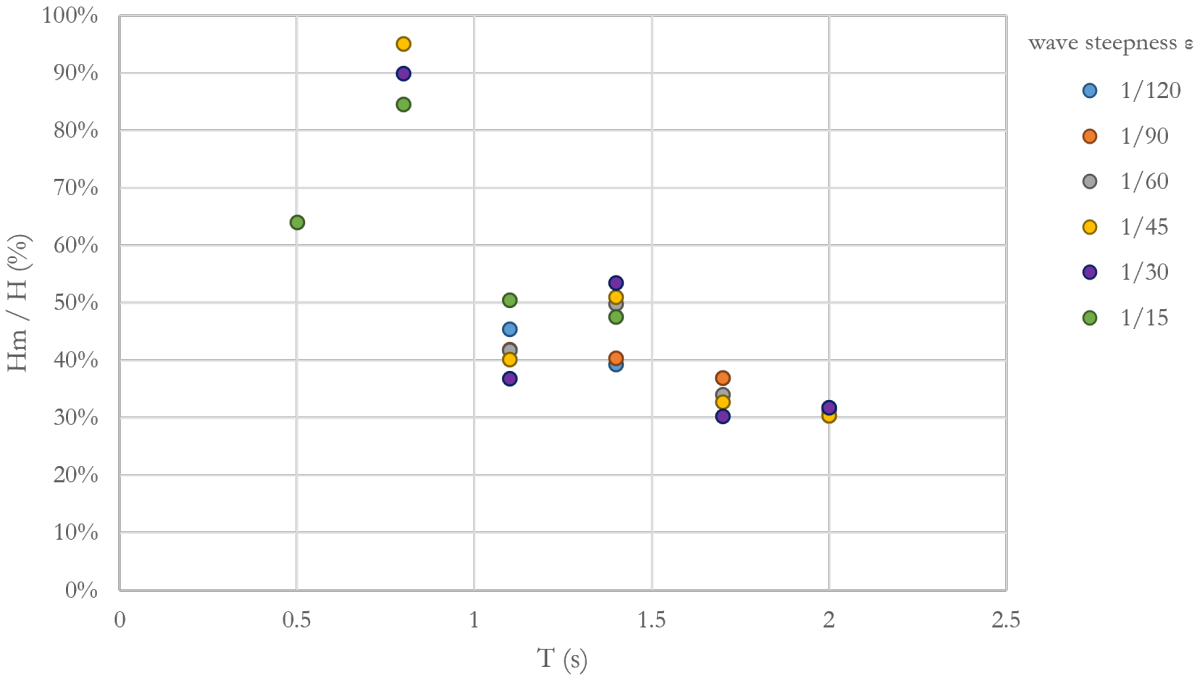

Figure 5.1 – Comparison of input to measured wave height

From the model tests, it can be concluded that conducting wave response experiments in the model tank at NTNU in Ålesund is possible. The frequency response characteristics of the model were obtained by creating a physical and digital model. The result is repeated in Figure 5.2. While none of the values in these two graphs correspond to each other, both results show a clear shape that corresponds to the theory on the response of floating structures. They start close to zero (mass-dominated), have a resonant peak, and follow the waves for higher periods (stiffness-dominated).

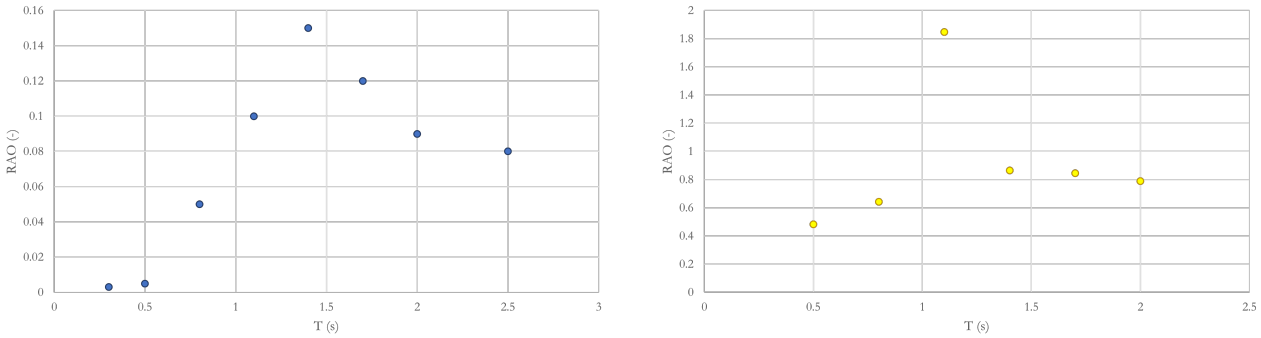

(a) Digital simulation

(b) Model tests

Figure 5.2 – Comparison of the RAO in vertical direction

5.2 Limitations

The wave tests showed that none of the waves reach their theoretical wave heights. Several limitations are identified which influence the wave environment in the tank:

- The wave flap itself is expected to be the main source of inaccuracies in the waves. The system that controls the wave flap was not investigated. Furthermore, the flow around the wave flap, shown in Figure 5.3, has an influence on the energy that is put into the waves. This effect was also not taken into account.
- Part of the second-order wave theory is that the amplitude should be included in the dispersion relation, where the relative amplitude affects the wave length. However, this was not done when defining the wave tests. Additionally, there is no way to measure the wave length, as there is only one wave probe that is set up.
- The fact that the wave probe is close to tank wall could cause measurement errors. The wall has friction effects which cause the wave propagation to be different. This effect was not measured or calculated, but can be seen visually. A diagram, where the curved lines show the front of the wave, is shown in Figure 5.4.

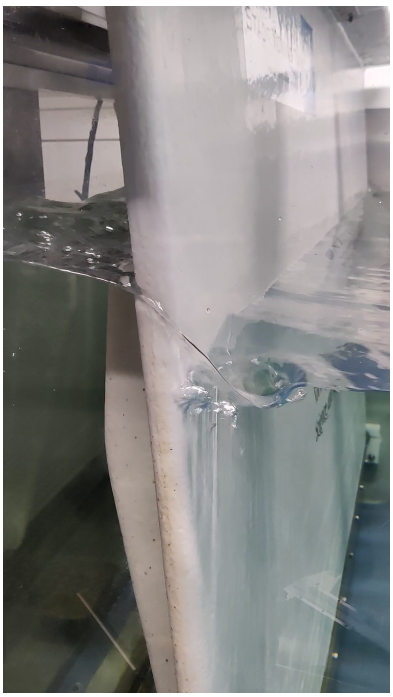

Figure 5.3 – Flow around the wave flap

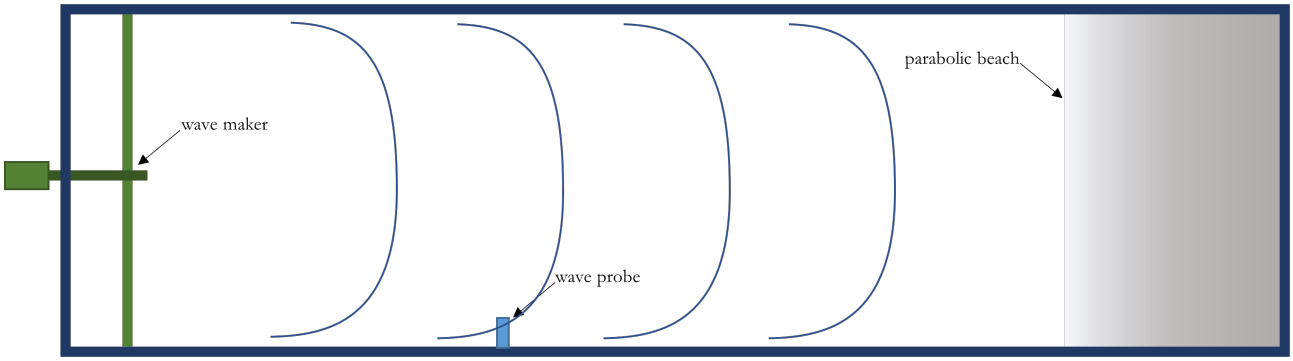

Figure 5.4 – Diagram of the wave propagation

The results model tests and digital simulation did not correspond to each other. Several limitations are identified which influence the motion response characteristics of the model:

- It is suspected the AquaSim software is not designed for simulations on model scale, even though these are possible and the simulations converge. This could cause a variety of numerical errors, which could explain the values obtained in this research.
- The mooring system used in the model tests consisted of chains, while in conventional fish farms a combination of chain and rope is used. This has both a different stiffness and mass, which influence the motion response of the model.
- The stiffness of the floaters and net was not calculated, however visually it was determined that both components were more stiff than they should to be able to compare to real fish farms.

5.3 Recommendations for future work

Further research into the wave environment and model tests is proposed:

- Expand the wave tests to include more periods, particularly around the suspected optimum.
- Install more wave probes to measure the wave length and wave propagation effects in the model tank.
- Examine the wave flap to determine if there are improvements that can be made in the control and flow.
- Set up a mooring system that is more representative of conventional solutions.
- Examine the stiffness and damping of the floaters and net of the model.
- Compare the model tests to a full-scale digital simulation and/or real-world data.

This page was left blank intentionally

References

Bannister, Raymond J. et al. (2016). "Near- and far-field dispersal modelling of organic waste from Atlantic salmon aquaculture in fjord systems". eng. In: *ICES journal of marine science* 73.9, pp. 2408–2419. ISSN: 1054-3139. DOI: 10.1093/icesjms/fsw027.

Berstad, Are J. (2022). *The Aquasim Package Theory User Manual*. Tech. rep. Aquastructures AS.

Faltinsen, Odd M. (1990). *Sea loads on ships and offshore structures*. eng. Cambridge ocean technology series. Cambridge: Cambridge University Press. ISBN: 0521372852.

Faltinsen, Odd M. and Yugao Shen (2018). "Wave and Current Effects on Floating Fish Farms: Keynote Contribution for the International Workshop on Wave Loads and Motions of Ships and Offshore Structures, Harbin, China, 5-7 November, 2017". In: *Journal of Marine Science and Application* 17. DOI: 10.1007/s11804-018-0033-5.

FAO (2022). *The State of World Fisheries and Aquaculture 2022*. FAO. ISBN: 978-92-5-136364-5. DOI: https://doi.org/10.4060/cc0461en.

Fiskeridirektoratet (2023). *NYTEK23: Forskrift om krav til teknisk standard for akvakulturanlegg for fisk i sjø, innsjø og vassdrag stiller minimumskrav til teknisk standard*. Online, accessed 01.05.2023. URL: https://www.fiskeridir.no/Akvakultur/Drift-og-tilsyn/nytek23.

Garlock, Taryn et al. (2020). "A Global Blue Revolution: Aquaculture Growth Across Regions, Species, and Countries". In: *Reviews in Fisheries Science and Aquaculture* 28.1, pp. 107–116. DOI: 10.1080/23308249.2019.1678111.

Hvas, Malthe, Ole Folkedal, and Frode Oppedal (2021). "Fish welfare in offshore salmon aquaculture". eng. In: *Reviews in aquaculture* 13.2, pp. 836–852. ISSN: 1753-5123. DOI: 10.1111/raq.12501.

Journée, J. M. J. and W. W. Massie (2001). *Offshore Hydromechanics*. Delft University of Technology. URL: https://ocw.tudelft.nl/wp-content/uploads/OffshoreHydromechanics_Journee_Massie.pdf.

MatWeb (n.d.). *MatWeb, Your Source for Materials Information*. Online, accessed 30.05.2023. n.d. URL: https://www.matweb.com/index.aspx.

Moe Føre, Heidi et al. (2022). "Technological innovations promoting sustainable salmon (Salmo salar) aquaculture in Norway". eng. In: *Aquaculture reports* 24, p. 101115. ISSN: 2352-5134. DOI: 10.1016/j.aqrep.2022.101115.

Mowi (n.d.). *Sea site - Press and media material*. Online, accessed 25.04.2023. n.d. URL: https://mowi.com/media/.

Mukhlas, Muhammad et al. (2021). "Bag and floater motions of a fabric membrane cage". In: *Journal of Fluids and Structures* 106, p. 103353. ISSN: 0889-9746. DOI: 10.1016/j.jfluidstructs.2021.103353.

Naylor, Rosamond L. et al. (2021). "A 20-year retrospective review of global aquaculture". In: *Nature* 591, pp. 551–563. URL: https://www.nature.com/articles/s41586-021-03308-6.

Qualisys AB (2022). *The QTM User Manual*. Tech. rep. Qualisys AB.

ScaleAQ (n.d.). *Pens - ScaleAQ*. Online, accessed 18.04.2023. n.d. URL: https://scaleaq.com/product-category/pen-net-and-mooring/pens/.

Standard Norge (2009). *NS9415:2009 Marine fish farms. Requirements for site survey, risk analyses, design, dimensioning, production, installation and operation.*

Standard Norge (2021). *NS9415:2021 Flytende Akvakulturanleg. Lokalisetsondersøkelse, prosjektering, utførelse og bruk.*

Whitham, Gerard B. (1999). *Linear and Nonlinear Waves*. John Wiley & Sons, Ltd. ISBN: 9781118032954. DOI: 10.1002/9781118032954.

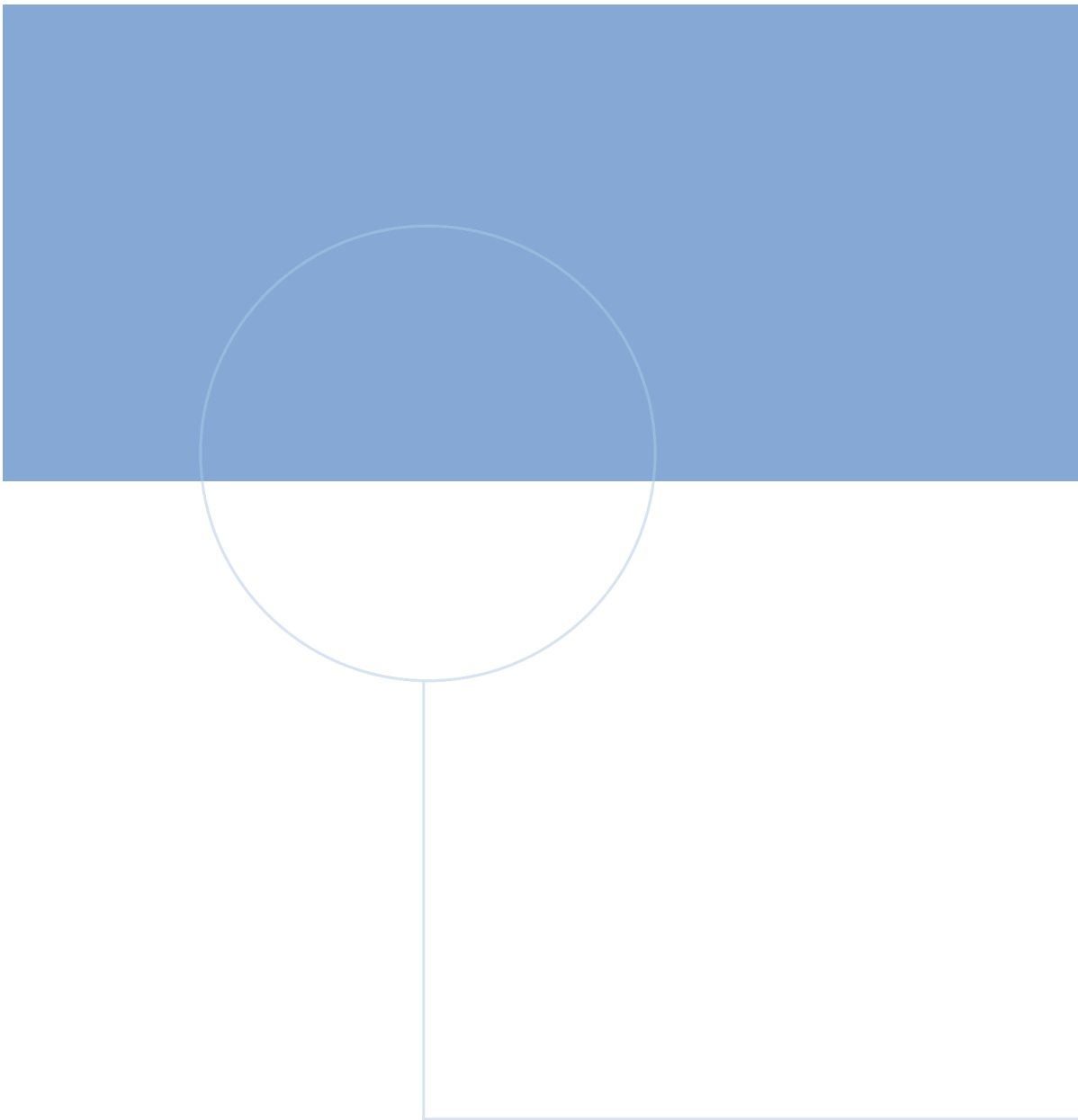

NTNU

Norwegian University of
Science and Technology